https://doi.org/10.5194/egusphere-2026-5912
Preprint. Discussion started: 11 November 2026
© Author(s) 2026. CC BY 4.0 License.

Transcontinental stratospheric and upper tropospheric measurements with the new GLORIA-Lite instrument

Gerald Wetzel[1], Felix Friedl-Vallon[1], Erik Kretschmer[1], Jörn Ungermann[2], Anne Kleinert[1], Tom Neubert[3], Peter Braesicke[1,a], Jan Cermak[1], Thomas Gulde[1], Michaela I. Hegglin[2,4,5], Michael Höpfner[1], Sören Johansson[1], Oliver Kirner[6], Guido Maucher[1], Christof Piesch[1], Peter Preusse[2], Markus Retzlaff[2], Michelle L. Santee[7], Georg Schardt[3], Roland Schmuker[1], Björn-Martin Sinnhuber[1], Wolfgang Woiwode[1], and Valéry Catoire[8]

[1]Institute of Meteorology and Climate Research Atmospheric Trace Gases and Remote Sensing (IMKASF), Karlsruhe Institute of Technology, Karlsruhe, Germany

[2]Institute of Climate and Energy Systems - Stratosphere (ICE-4), Forschungszentrum Jülich, Jülich, Germany

[3]Institute of Technology and Engineering (ITE), Forschungszentrum Jülich, Jülich, Germany

[4]Institute for Atmospheric and Environmental Research, University of Wuppertal, Wuppertal, Germany

[5]Department of Meteorology, University of Reading, Reading, UK

[6]Scientific Computing Center (SCC), Karlsruhe Institute of Technology, Karlsruhe, Germany

[7]Jet Propulsion Laboratory, California Institute of Technology, Pasadena, CA, USA

[8]Laboratoire de Physique et Chimie de l'Environnement et de l'Espace (LPC2E/CNRS), Université Orléans, Orléans, France

[a]now at: Business Area Research and Development, Deutscher Wetterdienst, Offenbach am Main, Germany

Correspondence to: Gerald Wetzel (gerald.wetzel@kit.edu)

Abstract

Accurate observations of the vertical distribution and temporal variability of atmospheric trace gases are essential for understanding atmospheric composition and chemistry and for evaluating atmospheric models. The Gimballed Limb Observer for Radiance Imaging of the Atmosphere (GLORIA) is a cooled limb-imaging Fourier-Transform Spectrometer (iFTS) providing mid-infrared spectra with high spectral resolution. The newly developed, compact and uncooled instrument GLORIA-Lite (GLITE) is significantly smaller and lighter than its predecessor GLORIA, thanks to recent advances in infrared sensors, tailored electronics, and innovative manufacturing technology. The first balloon version, GLITE-B, was deployed during a transcontinental stratospheric flight from Kiruna (Sweden) via Greenland to Canada in June 2024. Hyperspectral limb-emission measurements in the 750-1450 cm^{-1} spectral range were obtained from 22 to 24 June, covering an altitude range of 5 to 40 km. The observations were used to retrieve temperature and a wide range of ozone and other species involved in

https://doi.org/10.5194/egusphere-2026-5912
Preprint. Discussion started: 11 November 2026
© Author(s) 2026. CC BY 4.0 License.

stratospheric ozone chemistry, tracers of stratospheric air motions, and tropospheric air pollutants. Comparisons of the retrieved mean vertical volume mixing ratio (VMR) profiles with Microwave Limb Sounder (MLS) version 6 observations show good agreement over wide altitude ranges, with differences generally within the combined error limits and typically within ±2 K for temperature and ±10 % for O_3, HNO_3, and H_2O. A negative bias of approximately 20 % was found in the MLS N_2O data below 27 km relative to GLITE-B. Comparisons with the ECHAM5/MESSy Atmospheric Chemistry (EMAC) model indicate that the model successfully reproduces observed stratospheric trace-gas variability, chemistry ($ClONO_2$, NO_2, PAN), and transport characteristics (chlorofluorocarbons, SF_6) in the sunlit summer polar stratosphere, while discrepancies for HCOOH and CH_3OH highlight uncertainties in their sources and atmospheric processing. The CFC-11/CFC-12 tracer–tracer relationship agrees well with previous observations, and the observed SF_6 profiles are consistent with current understanding of stratospheric transport. The results of this first flight demonstrate that GLITE-B can provide accurate trace gas profiles with high vertical resolution during long-duration balloon flights. Such measurements capture the temporal evolution of atmospheric composition over several days, providing valuable information on transport and photochemical processes and supporting the evaluation and improvement of atmospheric chemistry models.

1 Introduction

Balloon-borne mid-infrared limb-emission measurements provide a well-established method for observing the spatial and temporal variability of trace gases in the upper troposphere and stratosphere, offering high vertical resolution below the instrument altitude, enabling the characterization of transport, photochemical processes, and the evolution of ozone-depleting and radiatively active gases (Fischer et al., 2008). In contrast to solar occultation techniques, limb-emission spectrometers are not dependent on an external radiation source and can therefore be operated under both daytime and nighttime conditions, enabling increased measurement flexibility (Friedl-Vallon et al., 2004). However, the use of cooled spectrometers involves increased technical complexity relative to uncooled systems. Consequently, stratospheric balloon missions employing such instruments were always limited to a small number (Carli et al., 1984; Murcray et al., 1984; Brasunas et al., 1988; Johnson et al., 1995). At the Karlsruhe Institute of Technology (KIT), the Michelson Interferometer for Passive Atmospheric Sounding (MIPAS) family of instruments was developed. In addition to an

https://doi.org/10.5194/egusphere-2026-5912
Preprint. Discussion started: 11 November 2026
© Author(s) 2026. CC BY 4.0 License.

airborne version, two balloon-borne MIPAS instruments (Fischer and Oelhaf, 1996; Friedl-Vallon et al., 2004) were deployed in numerous scientific campaigns between 1989 and 2014 (e.g. von Clarmann et al., 1993; Oelhaf et al., 1994; Wetzel et al., 1995; von Clarmann et al., 1997; Wetzel et al., 1997; Stowasser et al., 1999; Waibel et al., 1999; Höpfner et al., 2002; Stowasser et al., 2002, 2003; Wetzel et al., 2002; Wiegele et al., 2009; Wetzel et al., 2010, 2012, 2015, 2017). These instruments also served as precursors for the MIPAS Envisat satellite mission (Fischer et al., 2008) and played an essential role in its validation (e.g. Wetzel et al., 2022 and references therein) as well as in the validation of other satellite-based sensors such as the Global Ozone Monitoring by Occultation of Stars (GOMOS; Renard et al., 2008), the second Improved Limb Atmospheric Spectrometer (ILAS-II; Wetzel et al., 2006), and the Superconducting Submillimeter-Wave Limb-Emission Sounder (SMILES; Sagawa et al., 2013).

Limb-scanning spectrometers such as MIPAS typically require on the order of one minute to acquire a full vertical profile. In contrast, imaging spectrometers simultaneously measure all vertical geometries, enabling the retrieval of a full vertical profile from a single measurement and even achieve improved vertical resolution. This measurement concept was realized in the Gimballed Limb Observer for Radiance Imaging of the Atmosphere (GLORIA; Friedl-Vallon et al., 2014; Riese et al., 2014) as a joint project between KIT and the Forschungszentrum Jülich (FZJ). For observations extending into the middle stratosphere while retaining coverage down to the middle troposphere, the instrument was adapted for operation on a stratospheric balloon platform (Wetzel et al., 2025).

To further enhance flexibility in operation and deployment, a first lightweight, compact and uncooled version of GLORIA (called GLORIA-Lite or GLITE) was newly developed. The reduction in size and mass was achieved by eliminating the need for cooling of the instrument, reducing the spectral resolution, and using state-of-the-art infrared detector technology, dedicated electronics, and adapted manufacturing approaches. This instrument, specifically designed for balloon-borne measurements (hereafter referred to as GLITE-B), enabled the first transcontinental stratospheric flight from northern Sweden via Greenland to Canada in June 2024.

Here, we focus on the data analysis of the first imaging hyperspectral limb-emission dataset from 5 to 40 km altitude from GLITE-B during its initial deployment. We present selected retrieval results, including uncertainty estimates, altitude resolution, and comparisons of

https://doi.org/10.5194/egusphere-2026-5912
Preprint. Discussion started: 11 November 2026
© Author(s) 2026. CC BY 4.0 License.

temperature and long-lived tracer volume mixing ratios (VMRs) with Microwave Limb Sounder (MLS) observations. In addition, temporal and spatial variations of measured gases are compared with simulations from the chemistry-climate model ECHAM5/MESSy Atmospheric Chemistry (EMAC, Jöckel et al., 2010).

2 GLITE-B instrument, data analysis and modelling

The following subsections provide a brief overview of the GLITE-B instrument, a description of the data analysis and the atmospheric modelling used in this study.

2.1 GLITE-B instrument

The newly developed lightweight GLITE-B instrument, whose technical details will be published elsewhere, is an uncooled limb-imaging Fourier-Transform Spectrometer (iFTS) operating in the thermal infrared spectral region, covering wavelengths from approximately 7 to 14 µm. It uses a two-dimensional detector array that records 128 vertical and 47 horizontal interferograms per measurement. The interferograms are Fourier-transformed into the spectral domain and radiometrically calibrated using in-flight measurements of a blackbody and deep space, following an approach similar to that described by Wetzel et al. (2025). To improve the signal-to-noise ratio, spectra are averaged in the horizontal direction. As the vertical elevation coverage of a single image does not span the entire altitude range from the balloon at 40 km down to the upper troposphere, a toggle mode comprising eight consecutive measurements (four at upper and four at lower elevation angles) is applied. For the binned and combined datasets (100 s integration time), the noise equivalent spectral radiance (NESR) amounts to approximately 1 x 10^{-8} W (cm^2 sr cm^{-1})$^{-1}$. Spectra are recorded with a maximum optical path difference of 2.5 cm, corresponding to a spectral sampling of 0.2 cm^{-1}, and are apodized using the “strong” function of Norton and Beer (1976, 1977). These measurements enable the retrieval of numerous trace species, as individual spectral lines or the shape of the spectral band can be separated from continuum-like emissions.

2.2 Data analysis of measured spectra

In this study, we present results from the first GLITE-B balloon flight, carried out from Esrange (Kiruna, Sweden) via Greenland to Baffin Island (Canada) between 22 and 26 June 2024 as part of the transatlantic (CNES-TRANSAT) campaign. Due to a problem with the

https://doi.org/10.5194/egusphere-2026-5912
Preprint. Discussion started: 11 November 2026
© Author(s) 2026. CC BY 4.0 License.

interferometer drive, the measurements were terminated prematurely on 24 June 2024 near eastern Greenland. Figure 1 shows the flight trajectory and the corresponding measurement locations from 21:28 UTC on 22 June 2024 to 14:49 UTC on 24 June 2024.

Radiances are calculated with the Karlsruhe Optimized and Precise Radiative Transfer Algorithm (KOPRA; Stiller et al., 2002) using spectroscopic data from the high-resolution transmission molecular absorption database (HITRAN; Gordon et al., 2017). The retrieval is performed with the KOPRAFIT procedure (Höpfner et al., 2002), which employs derivatives of the radiance spectrum with respect to atmospheric state and instrument parameters (Jacobians) computed by KOPRA. The inverse problem is solved iteratively using a Gauss-Newton method (Nocedal and Wright, 2006) with Tikhonov-Phillips regularization (Phillips, 1962; Tikhonov, 1963), applied to the first derivative of the a priori profile of the retrieved atmospheric parameter. The retrieval grid is defined with a vertical spacing of 0.25 km up to 40 km altitude and becomes gradually coarser above, extending up to 100 km.

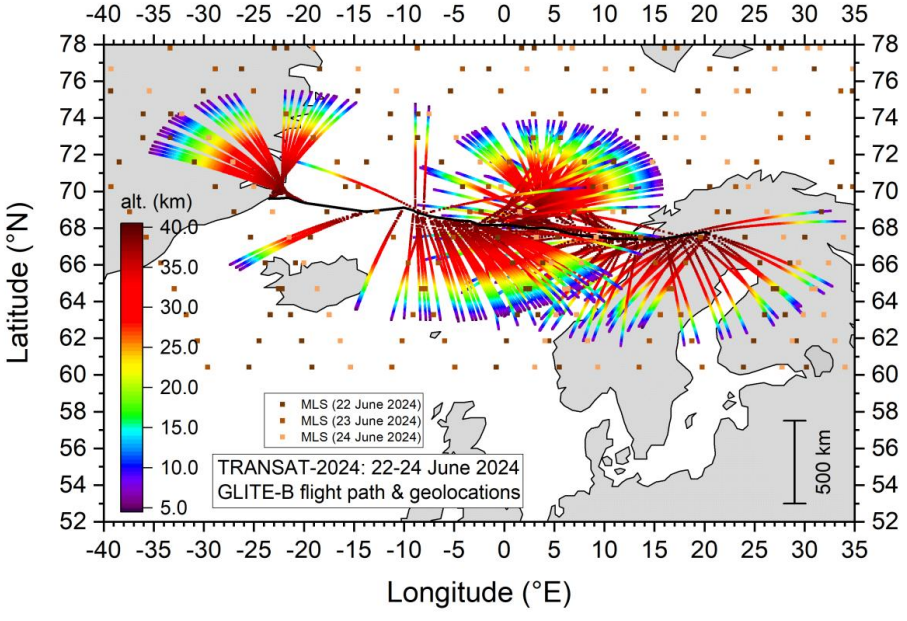


Figure 1. Flight path of the balloon gondola on 22-24 June 2024 (black line) and GLITE-B tangent point positions (colour-coded by altitude). Observations (north of 60 °N) of the Microwave Limb Sounder (MLS) are shown as brown squares.

https://doi.org/10.5194/egusphere-2026-5912
Preprint. Discussion started: 11 November 2026
© Author(s) 2026. CC BY 4.0 License.

Cloud-affected spectra are filtered using a cloud index threshold of 4, based on the colour ratio of the mean radiance in the spectral intervals 788.2-796.3 and 832.3-834.4 cm^{-1} (Spang et al., 2004). In a subsequent step, the pointing elevation angle is adjusted by performing a line of sight (LOS) retrieval using suitable CO_2 transitions in the spectral range 933.4-958.2 cm^{-1}, together with temperature profiles from European Centre for Medium-Range Weather Forecasts (ECMWF) ERA5 analyses (Hersbach et al., 2020). Prior to the trace gas retrievals, temperature is retrieved from the CO_2 Q-branch region near 792 cm^{-1} and the CO_2 laser band around 942 cm^{-1}. The retrieved temperature is subsequently used for the trace gas retrievals. The spectral windows applied for the GLITE-B retrieval of temperature and trace gases, along with the corresponding vertical resolution and estimated uncertainties, are summarized in Table 1. A careful selection of appropriate spectral windows is essential to ensure accurate retrievals. Major interfering species are fitted simultaneously with the target species, while minor species are either pre-fitted in separate spectral intervals or represented by climatological profiles during the retrieval. In the case of H_2O and O_3, a priori profiles are taken from ECMWF analyses for their retrievals, while the retrieved concentrations are included as fixed profiles in all subsequent trace gas retrievals.

The error estimation of the retrieved species includes contributions from random noise, temperature uncertainties, calibration (multiplicative gain), pointing (LOS), field of view (FOV) inaccuracies, and spectroscopic data errors; all errors refer to the 1-σ uncertainty.

2.3 Model simulations

A multi-year simulation was performed with the chemistry-climate model ECHAM5/MESSy Atmospheric Chemistry (EMAC). EMAC is a numerical chemistry and climate simulation system that includes submodels describing tropospheric and middle atmosphere processes and their interaction with oceans, land and human influences (Jöckel et al., 2010). Its core atmospheric model is the fifth-generation European Centre Hamburg general circulation model (ECHAM5; Roeckner et al., 2006) that is connected to the submodels using the interface Modular Earth Submodel System (MESSy). For this study, EMAC (MESSy v2.55.0) was run from 2019 to 2024 with a 4 min time step at T106L90 resolution (approximately 1.1° × 1.1°) and 90 hybrid pressure levels from the ground up to 0.01 hPa. Surface pressure, temperature, divergence, and vorticity up to an altitude of 1 hPa were nudged towards ECMWF ERA5 reanalysis data (Hersbach et al., 2020) to reproduce realistic synoptic conditions. The chemical mechanism comprises 137 gas-phase species, 261 gas-phase reactions, 80 photolysis reactions,

https://doi.org/10.5194/egusphere-2026-5912
Preprint. Discussion started: 11 November 2026
© Author(s) 2026. CC BY 4.0 License.

and 12 heterogeneous reactions. It includes tropospheric methane and non-methane hydrocarbon chemistry with C_1-C_5 organic compounds, including a condensed isoprene oxidation mechanism, as well as stratospheric and mesospheric chemistry. The rate constants of gas-phase reactions are from Atkinson et al. (2007), Sander et al. (2011), and Burkholder et al. (2015). Greenhouse gas and ozone-depleting substance (ODS) boundary conditions, including those for CO_2, CH_4, N_2O, chlorofluorocarbons, and halons, as well as emissions of non-methane volatile organic compounds (NMVOCs), are prescribed according to the Coupled Model Intercomparison Project Phase 6 (CMIP6; Eyring et al., 2016). For the time period of the balloon flight, the EMAC data were written out for each model timestep (every 4 minutes). These data were then interpolated in time and space onto the GLITE-B retrieval grid along the flight trajectory.

https://doi.org/10.5194/egusphere-2026-5912
Preprint. Discussion started: 11 November 2026
© Author(s) 2026. CC BY 4.0 License.

Table 1. Overview of GLITE-B spectral windows for retrieved quantities used in this study together with altitude resolution (alt. res.), typical noise errors and total errors, valid for a single vertical profile. Total errors include temperature uncertainties, calibration (multiplicative gain), pointing, field of view inaccuracies, and spectroscopic data errors.

Target quantity	Spectral range (cm^{-1})	Fitted atmospheric parameters	Alt. res. (km)	Noise error (%)	Total error (%)
Temp.	786.2 – 793.4 941.4 – 943.6	Temp.	< 2	0.2 – 0.3 K	0.5 – 1.0 K
O_3	763.6 – 767.4 780.6 – 784.0 784.8 – 789.6 991.0 – 997.8 999.2 – 1002.6	O_3	< 2	1 – 5	7 – 10
H_2O	824.0 – 830.2 1214.2 – 1220.0 1393.6 – 1406.0 1416.6 – 1425.2	H_2O, O_3, CH_4	< 2	2 – 4	10 – 20
N_2O	1215.4 – 1217.0 1227.6 – 1229.0 1229.8 – 1235.4 1278.0 – 1279.8 1289.4 – 1292.0	N_2O, CH_4	< 2	1 – 10	8 – 30
CFC-11	831.0 – 832.0 845.0 – 849.8 850.0 – 854.6 854.8 – 859.4 862.2 – 862.6	H_2O, HNO_3, $COCl_2$, CFC-11	< 2	1 – 10	5 – 15
CFC-12	918.2 – 924.2	HNO_3, CFC-12	< 2	1 – 10	6 – 15
SF_6	945.2 – 950.4	H_2O, SF_6	< 4	4 – 8	10 – 20
HNO_3	860.2 – 864.0 866.0 – 870.2 872.2 – 880.0 892.6 – 901.8	HNO_3	< 2	1 – 4	20 – 25*
$ClONO_2$	778.2 – 781.6	O_3, $ClONO_2$	< 2	10 – 20	15 – 25
NO_2	801.0 – 820.0	H_2O, O_3, NO_2, HNO_3, COF_2, HCFC-22, CCl_4, CFC-113, $ClONO_2$, HNO_4, PAN, $BrONO_2$	< 8	5 – 15	7 – 20
PAN	779.8 – 805.4	H_2O, O_3, HCFC-22, CCl_4, PAN	< 2	5 – 15	10 – 30
CH_3OH	960.0 – 999.4	O_3, NH_3, CH_3OH, PAN	< 2	6 – 25	8 – 30
HCOOH	1086.4 – 1089.6 1103.4 – 1106.2 1112.4 – 1117.0	O_3, HCOOH, CFC-12, HCFC-22	< 2	7 – 20	10 – 40

*Large spectroscopic error.

https://doi.org/10.5194/egusphere-2026-5912
Preprint. Discussion started: 11 November 2026
© Author(s) 2026. CC BY 4.0 License.

3 Results

3.1 Comparison of GLITE-B measurements with observations and EMAC model data

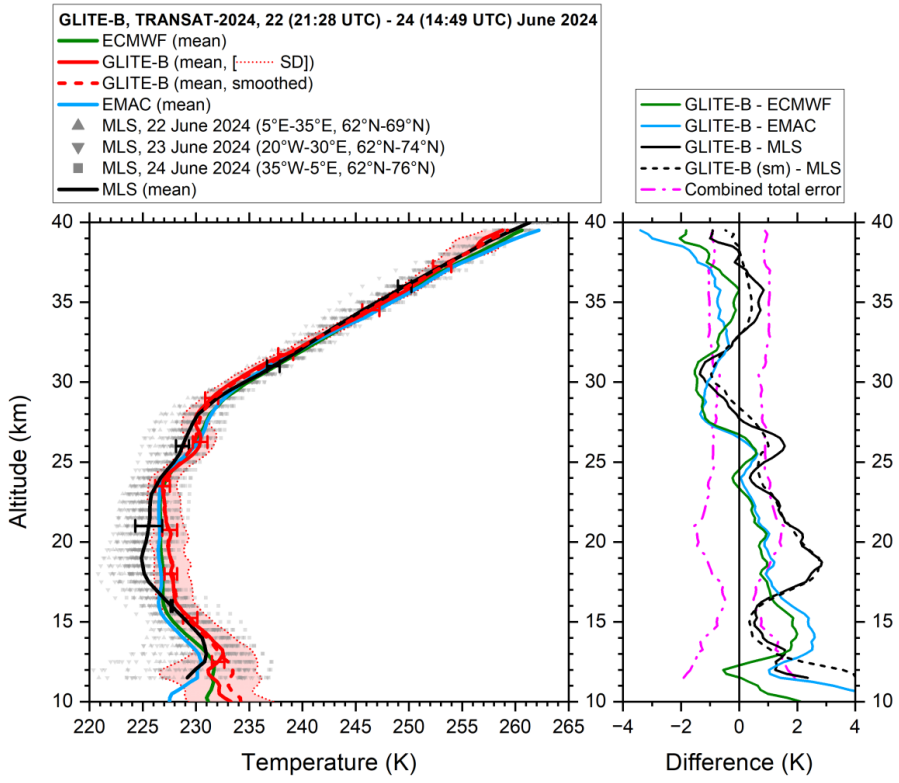
In this section, mean vertical profiles of temperature, O_3, HNO_3, H_2O, and N_2O from GLITE-B retrievals (averaged over the entire balloon flight) are compared to MLS (Waters et al., 2006; Santee et al., 2011) observations and EMAC simulations. The comparison of mean profiles has the advantage that the noise component of the error is reduced by a factor of $1/n^{0.5}$ where n denotes the number of averaged data points. To assess whether a bias between the instruments is statistically significant, combined uncertainties (random and systematic) are calculated as the square root of the sum of the squared individual measurement uncertainties, following Wetzel et al. (2022). Since the vertical resolution of GLITE-B profiles is substantially higher than that of MLS, the GLITE-B retrieval was repeated using a stronger regularization (smoothing) to obtain a vertical resolution comparable to that of MLS. To calculate differences, all data shown in the following figures were interpolated onto the GLITE-B retrieval grid.

3.1.1 Temperature

Apart from its role as a primary atmospheric state variable, accurate temperature profiles are essential for reliable trace gas retrievals from atmospheric emission limb soundings, as temperature errors propagate into the retrieved abundances and their overall uncertainty. Figure 2 presents the mean temperature profile observed by GLITE-B between 21:28 UTC on 22 June 2024 and 14:49 UTC on 24 June 2024, together with MLS version 6 profiles (Schwartz et al., 2026b) and mean temperatures from ECMWF ERA5 analyses (Hersbach et al., 2020) interpolated onto the GLITE-B retrieval grid. The corresponding mean temperature profile simulated by EMAC and sampled at GLITE-B measurement geolocations, is also shown.

Mean temperature differences between GLITE-B and MLS remain within the combined uncertainties over broad altitude ranges above 10 km and are generally smaller than 2 K. A positive bias of GLITE-B relative to MLS is evident below 27 km, reaching up to 3 K at 19 km. This is consistent with previously reported deviations between MLS and other satellite instruments (Livesey et al., 2026). The pronounced deviation between GLITE-B and MLS at 26 km is reduced when the smoothed GLITE-B profile is compared with MLS. A small positive bias of GLITE-B relative to ECMWF and EMAC is evident below 26 km, whereas a slight negative bias is found above 26 km.

https://doi.org/10.5194/egusphere-2026-5912
Preprint. Discussion started: 11 November 2026
© Author(s) 2026. CC BY 4.0 License.



245 **Figure 2.** Left: Mean GLITE-B temperature profile (red solid line, including total error and standard deviation, SD); GLITE-B smoothed (vertical resolution comparable to that of MLS, red dashed line); MLS version 6 data points (grey symbols), mean MLS vertical profile (black solid line with total error), mean ECMWF profile (green solid line), and mean EMAC profile (blue solid line). Right: Absolute differences together with combined total error of GLITE-B and MLS.

250

3.1.2 O_3

Monitoring the anticipated recovery of the stratospheric ozone (O_3) layer remains an important scientific objective (Chipperfield and Bekki, 2024; WMO, 2022). Continuous ozone observations are further required because ozone acts as an effective greenhouse gas in the upper
255 troposphere and lower stratosphere (UTLS), where it contributes to the radiative budget (Forster and Shine, 1997; Gettelman et al., 2011; Hansen et al., 1997; Riese et al., 2012; Xie et al., 2008). Figure 3 shows the mean ozone profile retrieved from GLITE-B spectra together with MLS version 6 profiles (Schwartz et al., 2026a), corresponding ozone profiles from ECMWF ERA5 analyses (Hersbach et al., 2020) and EMAC simulations. Differences between the mean O_3
260 profiles from GLITE-B and MLS remain within the combined error limits throughout the entire

https://doi.org/10.5194/egusphere-2026-5912
Preprint. Discussion started: 11 November 2026
© Author(s) 2026. CC BY 4.0 License.

altitude range, although a small, statistically insignificant bias of less than 10 % is apparent above 20 km. The pronounced VMR peak observed by GLITE-B at 26 km appears to represent a genuine dynamical feature rather than a retrieval artefact, as it is evident both in the measurements and in the EMAC simulation. Applying stronger regularization (smoothing) to the GLITE-B retrieval indeed reduces the amplitude of the peak, resulting in a profile shape that more closely resembles the MLS observations. Figure 4a shows the two-dimensional O_3 distribution observed by GLITE-B in comparison with the EMAC simulation shown in Fig. 4b. The secondary O_3 maximum at an altitude of approximately 26 km is clearly visible in both the measurements and the simulation. Small-scale temporal variations are correlated with changes in the azimuth angle of the line of sight. Figure 4c presents the horizontal O_3 distribution at around 26 km as simulated by EMAC. A dynamical structure with enhanced O_3 values is visible along the flight path of the balloon gondola. The high vertical resolution of GLITE-B enables the resolution of such dynamical features. The close agreement between EMAC and GLITE-B also indicates a realistic representation of atmospheric transport and supports the successful nudging of the model to meteorological reanalyses.

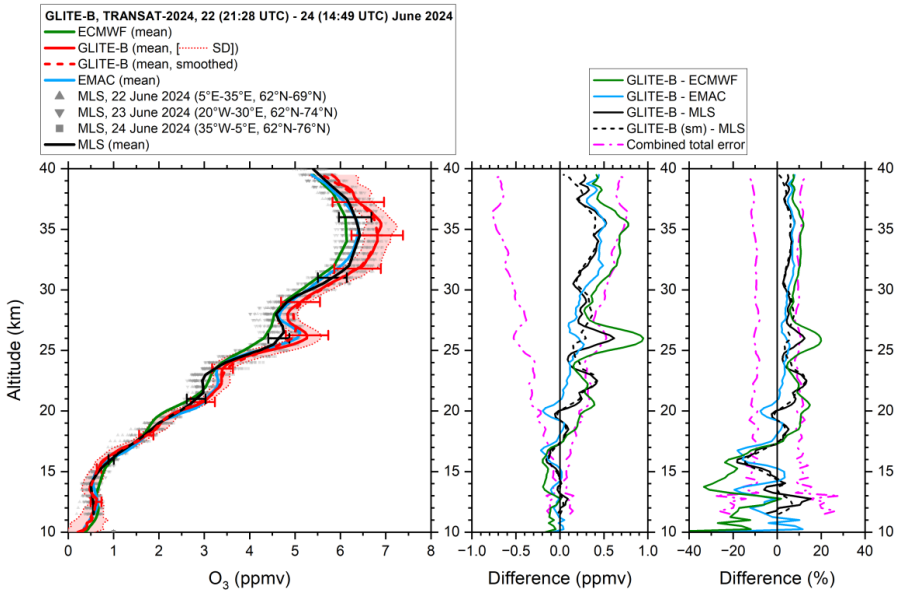


Figure 3. Left: Mean GLITE-B O_3 profile (red solid line, including total error and standard deviation, SD); GLITE-B smoothed (vertical resolution comparable to that of MLS, red dashed line); MLS version 6 data points (grey symbols), mean MLS vertical profile (black solid line with total error), mean ECMWF profile (green solid line), and mean EMAC profile (blue solid line). Middle and right: Absolute and relative differences together with combined total error of GLITE-B and MLS.

https://doi.org/10.5194/egusphere-2026-5912
Preprint. Discussion started: 11 November 2026
© Author(s) 2026. CC BY 4.0 License.

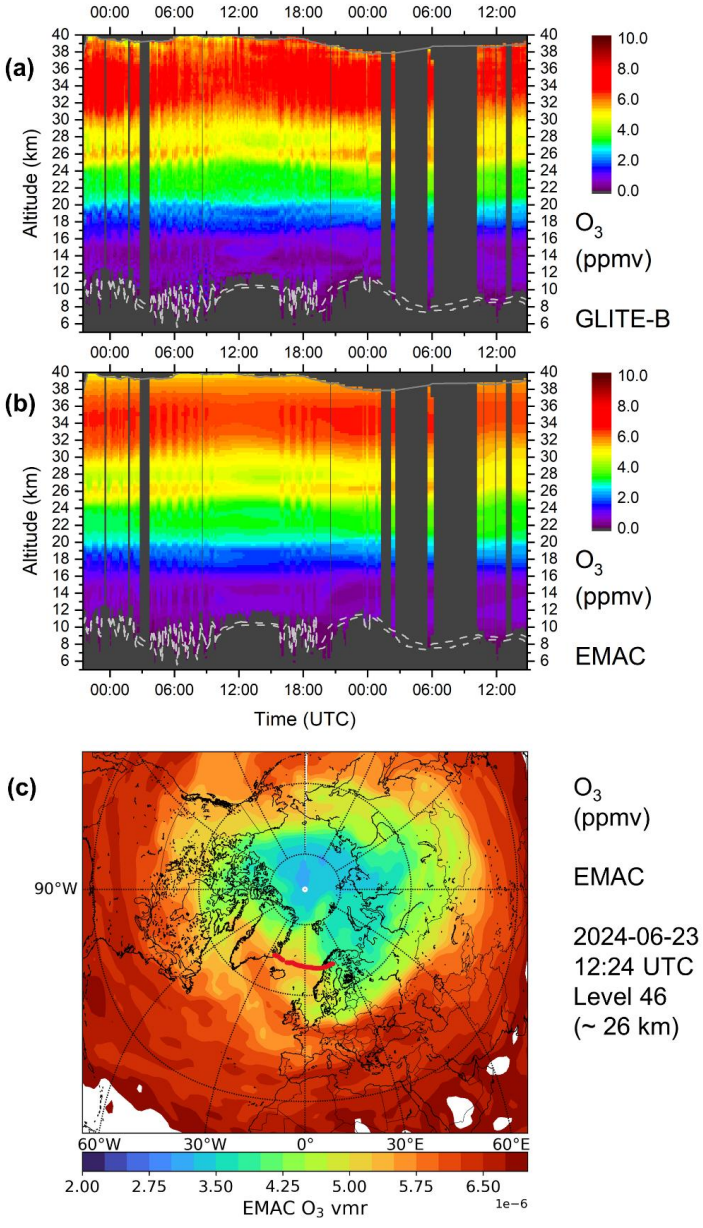


Figure 4. Temporal evolution of O_3 observed by GLITE-B between 22 and 24 June 2024 above the North Atlantic **(a)**. The flight altitude is shown as a solid grey line. The dynamical tropopause using ECMWF 2 and 4 potential vorticity (PV) units is indicated as dashed grey lines. The corresponding EMAC simulation **(b)**, together with the horizontal O_3 distribution from EMAC at about 26 km **(c)**, including the balloon flight trajectory during the GLITE-B observations (red line between northern Scandinavia and eastern Greenland).

https://doi.org/10.5194/egusphere-2026-5912
Preprint. Discussion started: 11 November 2026
© Author(s) 2026. CC BY 4.0 License.

3.1.3 HNO_3

Nitric acid (HNO_3) is an important reservoir species of reactive nitrogen in the stratosphere (e.g. Brasseur and Solomon, 2005). The mean GLITE-B HNO_3 profile is shown in Fig. 5. Because the uncertainty of the GLITE-B retrieval is dominated by spectroscopic uncertainties, primarily line intensity and pressure-broadening parameters from the HITRAN database (Gordon et al., 2017, 2022, 2026), an additional combined error estimate was calculated excluding the spectroscopic contribution. The differences between the mean GLITE-B and MLS version 6 HNO_3 profiles (Manney et al., 2026) remain within this reduced combined error, indicating that the observed VMR differences are not statistically significant. The secondary maximum observed by GLITE-B at 11 km, which is also apparent in the vertically smoothed GLITE-B profile, is likewise captured by MLS. The EMAC simulations are in close agreement with the GLITE-B observations and also reproduce the enhanced HNO_3 concentrations at 11 km.

Figure 6a shows the two-dimensional HNO_3 distribution observed by GLITE-B in comparison with the EMAC simulation shown in Fig. 6b. The pronounced, time-invariant stratospheric HNO_3 maximum, with values of around 8 ppbv, is clearly observed in both the measurements and the model simulations. In the lowermost stratosphere below 15 km, however, stronger HNO_3 variability is found, depending on the specific measurement location along the balloon flight trajectory. This variability is also reproduced by the EMAC simulation, although not always at exactly the same locations. Figure 6c shows the horizontal HNO_3 distribution as simulated by EMAC at an altitude of about 11 km. Here, fragments of HNO_3-rich air are visible, which are most likely remnants of polar vortex air from the previous Arctic winter, consistent with observations of similar HNO_3-rich fragments reported by Santee et al. (2011). This pattern likely explains the observed HNO_3 variability in the lowermost stratosphere.

https://doi.org/10.5194/egusphere-2026-5912
Preprint. Discussion started: 11 November 2026
© Author(s) 2026. CC BY 4.0 License.

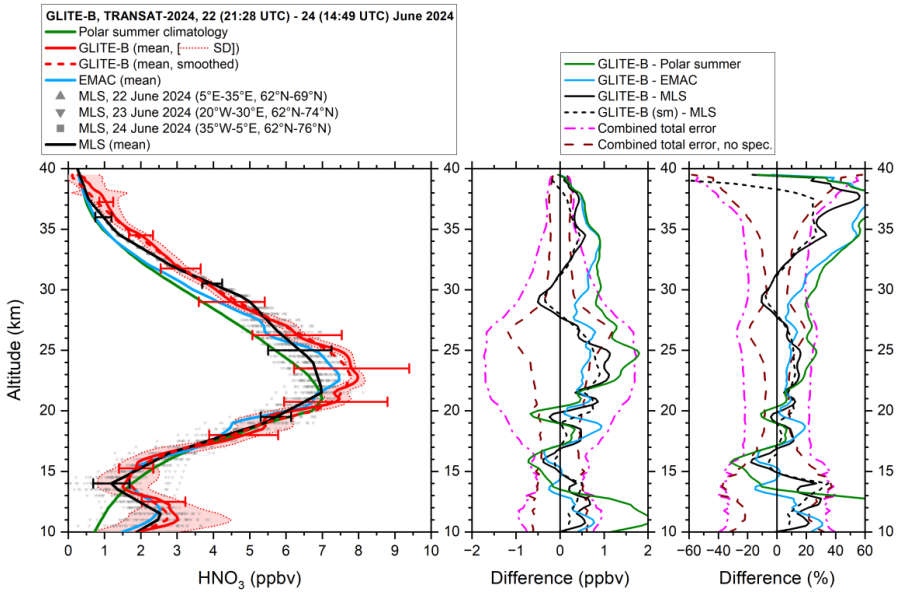
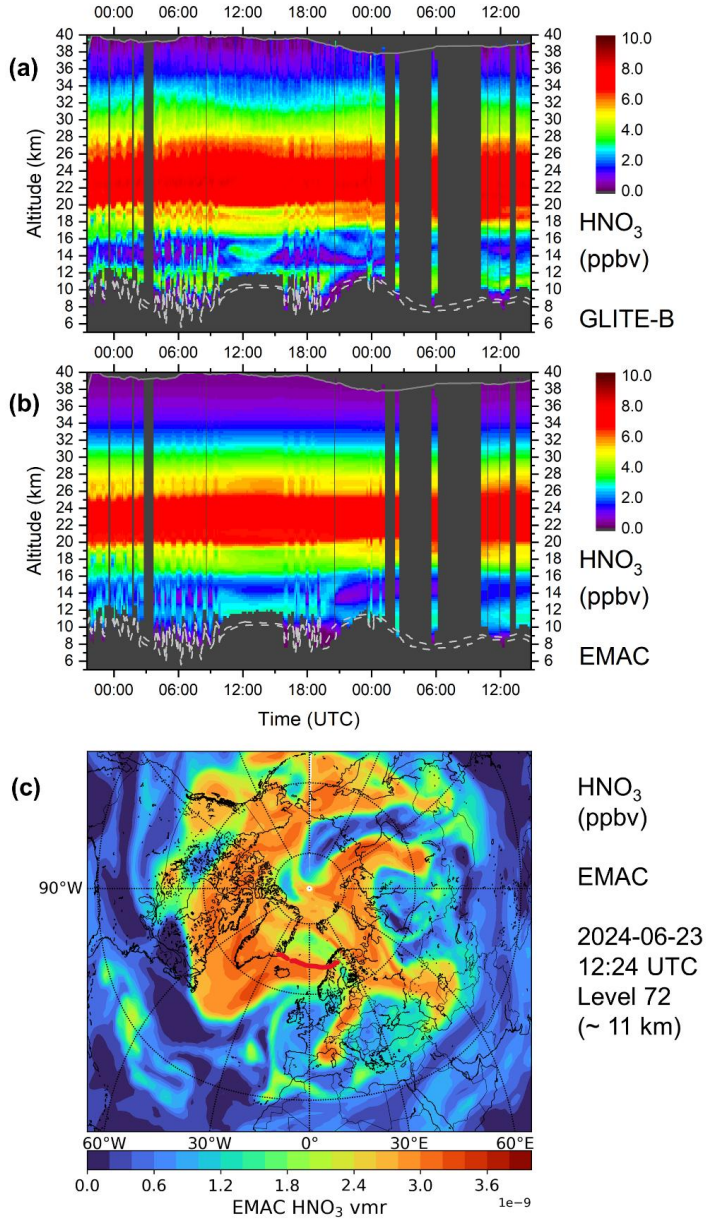


Figure 5. Left: Mean GLITE-B HNO_3 profile (red solid line, including total error and standard deviation, SD); GLITE-B smoothed (vertical resolution comparable to that of MLS, red dashed line); MLS version 6 data points (grey symbols), mean MLS vertical profile (black solid line with total error), a climatological polar summer profile (green solid line; Remedios et al., 2007), and mean EMAC profile (blue solid line). Middle and right: Absolute and relative differences together with combined total error of GLITE-B and MLS (with and without GLITE-B spectroscopic uncertainties).

https://doi.org/10.5194/egusphere-2026-5912
Preprint. Discussion started: 11 November 2026
© Author(s) 2026. CC BY 4.0 License.



320 **Figure 6.** Temporal evolution of HNO_3 observed by GLITE-B between 22 and 24 June 2024 above the North Atlantic **(a)**. The flight altitude is shown as a solid grey line. The dynamical tropopause using ECMWF 2 and 4 potential vorticity (PV) units is indicated as dashed grey lines. The corresponding EMAC simulation **(b)**, together with the horizontal HNO_3 distribution from EMAC at about 11 km **(c)**, including the balloon flight trajectory during the GLITE-B observations (red line between northern Scandinavia and eastern Greenland).

325

https://doi.org/10.5194/egusphere-2026-5912
Preprint. Discussion started: 11 November 2026
© Author(s) 2026. CC BY 4.0 License.

3.1.4 H_2O

Water vapour (H_2O) is a highly variable atmospheric constituent that plays a key role in the atmospheric energy budget. In the UTLS region, H_2O strongly influences the outgoing long-wave radiation and the Earth's radiation budget (e.g. Forster and Shine, 2002; Riese et al., 2012; Solomon et al., 2010). Accurate atmospheric H_2O measurements are therefore essential for assessing long-term trends (e.g. Dessler et al., 2014; Khosrawi et al., 2018; Lossow et al., 2018), particularly in the light of the Hunga volcanic eruption, which introduced a significant amount of water vapour into the stratosphere (Zhu et al., 2025).

Figure 7 shows the mean H_2O profile observed by GLITE-B together with MLS version 6 profiles (Lambert et al., 2026b) as well as corresponding H_2O profiles from ECMWF ERA5 analyses (Hersbach et al., 2020) and EMAC simulations. Due to the reduced number of MLS H_2O observations resulting from the duty cycling of the 190-GHz subsystem since May 2024 (Livesey et al., 2026), no MLS H_2O measurements were available at the location and time of the balloon flight. Therefore, backward trajectories were used to identify a region where the air mass sampled by GLITE-B had previously been observed by MLS at times MLS H_2O data are available, allowing a comparison between MLS and GLITE-B observations. Differences between the mean H_2O profiles from GLITE-B and MLS remain within the combined uncertainties throughout the entire altitude range, although a positive bias of 10–20 % is apparent in the GLITE-B data between 14 and 29 km. Below the hygropause, the strong vertical H_2O gradient results in larger differences between the two instruments. While ozone exhibits a pronounced VMR peak at 26 km, a distinct H_2O dip is observed at this altitude. When applying stronger regularization to the GLITE-B retrieval, resulting in a vertical resolution comparable to that of MLS, the mean profiles of the two instruments become more similar in shape. The VMR dip is evident not only in the measurements but also in the EMAC simulation. A clear negative bias of about 1 ppmv is visible in the EMAC (and ECMWF) profiles relative to the GLITE-B and MLS observations above 28 km. Relative to GLITE-B, this negative bias in EMAC persists down to 12 km (and down to 17 km for ECMWF). The negative bias of approximately 1 ppmv above 28 km may partly reflect the absence of the persistent Hunga H_2O anomaly in the EMAC simulation. Satellite observations indicate that the excess stratospheric H_2O injected by the January 2022 eruption persisted through at least early 2024 and remained of the order of 1 ppmv over large parts of the stratosphere (Millán et al., 2024).

https://doi.org/10.5194/egusphere-2026-5912
Preprint. Discussion started: 11 November 2026
© Author(s) 2026. CC BY 4.0 License.

Figure 8a shows the two-dimensional H_2O distribution observed by GLITE-B in comparison with the EMAC simulation shown in Fig. 8b. The H_2O VMR minimum at 26 km is clearly resolved by both the high-vertical-resolution GLITE-B observations and the EMAC simulation. It is also evident in the simulated horizontal H_2O distribution at around 26 km along the balloon flight path (Fig. 8c). The observed anticorrelation between H_2O and O_3 at 26 km is consistent with a dynamical origin of the observed feature, reflecting differences in the transport history of the air masses reaching this altitude rather than a direct chemical coupling between H_2O and O_3.

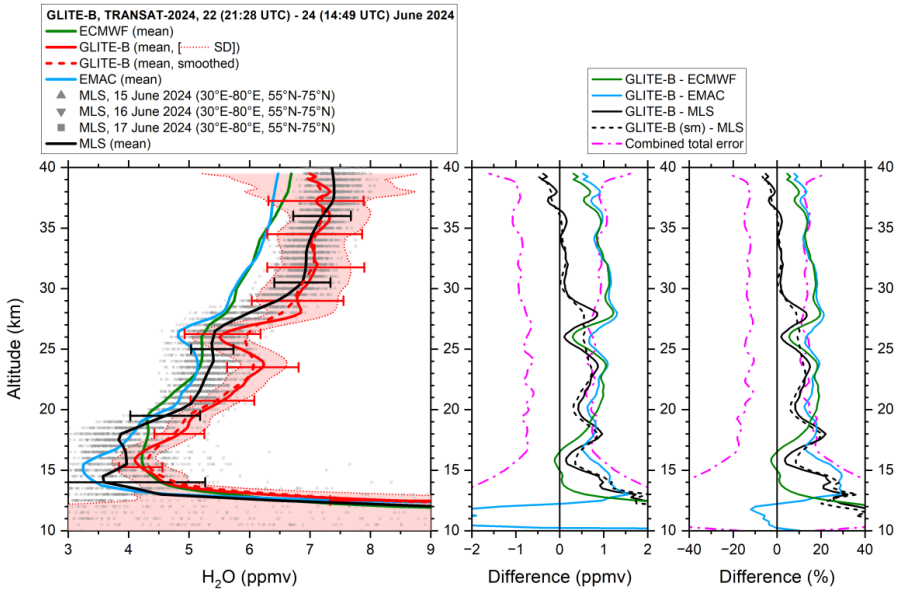
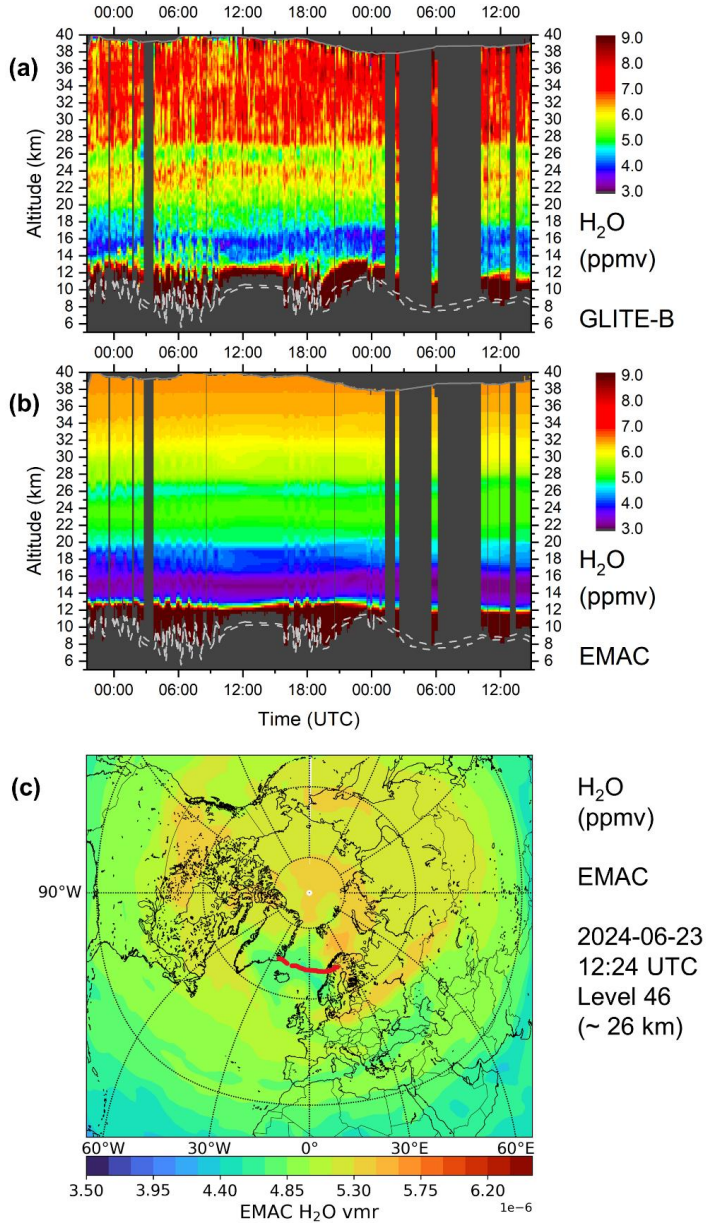


Figure 7. Same as Fig. 3 but for H_2O, with MLS observations corresponding to different times and locations (for details, see text).

https://doi.org/10.5194/egusphere-2026-5912
Preprint. Discussion started: 11 November 2026
© Author(s) 2026. CC BY 4.0 License.



370 **Figure 8.** Same as Fig. 4 but for H_2O.

https://doi.org/10.5194/egusphere-2026-5912
Preprint. Discussion started: 11 November 2026
© Author(s) 2026. CC BY 4.0 License.

3.1.5 N_2O

Nitrous oxide (N_2O) is a long-lived tracer of tropospheric origin. It is destroyed in the stratosphere by photolysis and reaction with $O(^1D)$, resulting in a vertical decrease of its mixing ratio with altitude (Brasseur and Solomon, 2005). Figure 9 shows the mean N_2O profile retrieved from GLITE-B spectra together with MLS version 6 profiles (Lambert et al., 2026a) and corresponding EMAC simulations. As for H_2O, no MLS measurements were available at the time and location of the balloon flight; therefore, MLS observations from the same air-mass region as used for H_2O were employed for the comparison with GLITE-B. Above 27 km, excellent agreement is found between MLS and GLITE-B. As in the case of O_3 and H_2O at 26 km, a dynamical feature is also evident in the GLITE-B N_2O profile, which is smoothed out when degrading the GLITE-B retrieval to the vertical resolution of MLS. Below 27 km, a significant bias of roughly 20 % is observed between MLS and GLITE-B, which slightly exceeds the combined total error estimate. This apparent negative bias in MLS N_2O is consistent with previously reported deviations between MLS and other satellite instruments (Livesey et al., 2026). However, EMAC-simulated N_2O values are close to the GLITE-B profile and also reproduce the VMR enhancement at 26 km. The climatological polar summer profile, based on Remedios et al. (2007) and adjusted to current values following Ungermann et al. (2022), lies within the range of the other profiles shown here.

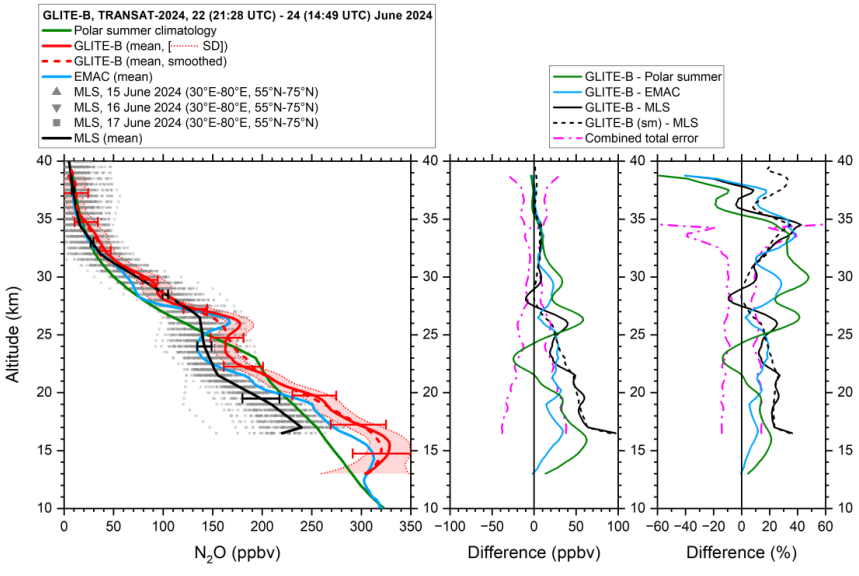


Figure 9. Same as Fig. 7, but for N_2O, with a polar summer climatological profile shown instead of the ECMWF profile.

https://doi.org/10.5194/egusphere-2026-5912
Preprint. Discussion started: 11 November 2026
© Author(s) 2026. CC BY 4.0 License.

3.2 GLITE-B measurements and EMAC simulations

In this section, we demonstrate that GLITE-B can resolve temporal changes in the mixing ratios of the photochemically active nitrogen and chlorine species NO_2 and $ClONO_2$ with high spatial and temporal resolution. Balloon-borne observations are particularly well suited for studying the diurnal variability of these species, as the balloon drifts with the surrounding air and repeatedly samples essentially the same air mass. Such measurements are also valuable for investigating the impact of episodic pollution events, such as biomass-burning plumes. The increasing extent and intensity of biomass-burning and wildfire events (e.g. Potapov et al., 2025) can enhance pollution in the upper troposphere through rapid vertical transport, while the relatively long atmospheric lifetimes of many trace gases and strong winds in this region allow them to be transported over large distances under favourable atmospheric conditions (e.g. Alvarado et al., 2020; Johansson et al., 2022; Lu et al., 2019). Another important application is the determination of the age of air, a commonly used diagnostic of the strength of the Brewer-Dobson circulation (e.g. Waugh and Hall, 2002). Sulphur hexafluoride (SF_6) and chlorofluorocarbons (CFCs) are key tracers for estimating the mean age of air (Voet et al., 2025). These long-lived compounds are transported into the stratosphere, where CFCs are gradually destroyed by photolysis. Their degradation ultimately releases inorganic chlorine, which, following temporary sequestration in reservoir species, contributes to catalytic ozone depletion in the polar spring (e.g. Brasseur and Solomon, 2005). In the following, we present examples of these trace species together with corresponding EMAC simulations.

3.2.1 $ClONO_2$ and NO_2

Chlorine nitrate ($ClONO_2$) is an important reservoir species in stratospheric chemistry, particularly with regard to ozone depletion (e.g. Brasseur and Solomon, 2005; von Clarmann and Johansson, 2018). It acts as a temporary reservoir for reactive chlorine, thereby reducing the availability of chlorine species involved in catalytic ozone-destruction cycles. A small diurnal variation of stratospheric $ClONO_2$ was already measured by the MIPAS balloon instrument during the Arctic winter in January 2010 (Wetzel et al., 2012). The temporal variation of $ClONO_2$ retrieved from the GLITE-B measurements is shown in Fig. 10a. Mixing ratios of up to 1.0 ppbv are observed. At the highest altitude levels, some noise-related structures are visible, likely caused by the lower signal-to-noise ratio in this altitude region. $ClONO_2$ exhibits some diurnal variability at altitudes above about 22 km, reflecting the balance between its production from NO_2 and ClO and its loss by photolysis. Consequently, $ClONO_2$

https://doi.org/10.5194/egusphere-2026-5912
Preprint. Discussion started: 11 November 2026
© Author(s) 2026. CC BY 4.0 License.

425 VMRs are slightly enhanced at high solar zenith angles (SZAs) compared with periods of low SZA. Superimposed on this diurnal signal, short-term fluctuations in the retrieved $ClONO_2$ VMR are associated with azimuthal rotations of the instrument. The EMAC simulation reproduces the observed variability with a slightly weaker diurnal amplitude (Fig. 10b). This leads to small deviations between simulated and measured $ClONO_2$ VMRs above about 25 km.

430 At lower altitudes, however, where no significant diurnal variability is apparent, the agreement between measurements and simulations is generally good, and the differences remain small (Fig. 10c).

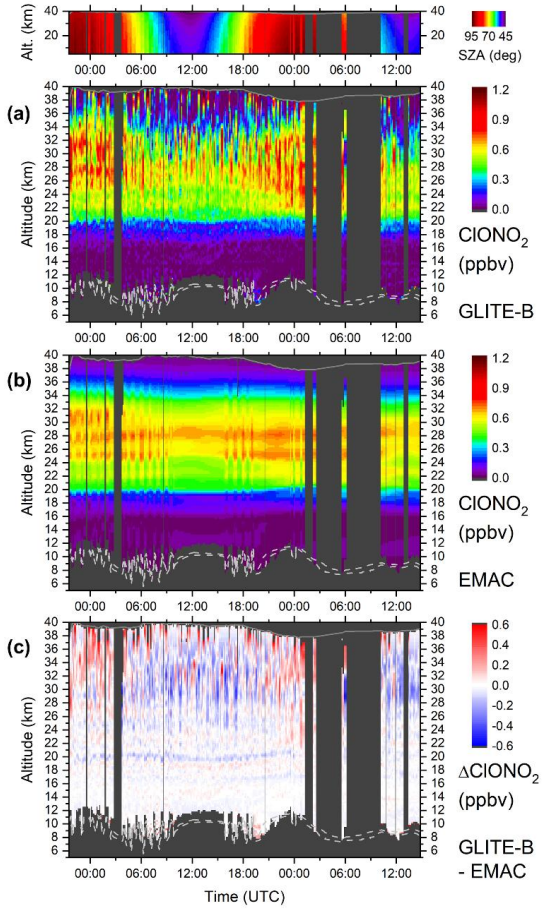


Figure 10. Temporal evolution of $ClONO_2$ observed by GLITE-B between 22 and 24 June 2024 above the
435 North Atlantic **(a)**. The solar zenith angle (SZA) is indicated at the top and applies to all panels. The flight altitude is shown as a solid grey line. The dynamical tropopause using ECMWF 2 and 4 potential vorticity (PV) units is indicated as dashed grey lines. The corresponding EMAC simulation **(b)** and the difference between the measurement and the model results **(c)** are also shown.

https://doi.org/10.5194/egusphere-2026-5912
Preprint. Discussion started: 11 November 2026
© Author(s) 2026. CC BY 4.0 License.

Nitrogen dioxide (NO_2) exhibits a pronounced diurnal cycle, with higher mixing ratios during the night than during the day, owing to its strong photochemical coupling with NO in the stratosphere (Brasseur and Solomon, 2005). Although NO_2 also participates in the N_2O_5 diurnal cycle, this pathway is negligible under polar day conditions. GLITE-B measurements show N_2O_5 mixing ratios below 0.1 ppbv throughout the flight (not shown), remaining below the detection limit. Pronounced diurnal variations of NO_2 have previously been observed by the MIPAS balloon instrument during Arctic winter over northern Scandinavia (Wetzel et al., 2012; Wiegele et al., 2009). Figure 11a shows the temporal evolution of the NO_2 volume mixing ratio measured by GLITE-B during the 2024 polar summer balloon flight. NO_2 mixing ratios of up to 9.2 ppbv were observed. As the sampled air masses above 10 km remained continuously sunlit, the diurnal variation is much weaker than under alternating day and night conditions. Nevertheless, higher NO_2 mixing ratios coincide with larger SZAs, and vice versa. A similar temporal evolution is evident in the EMAC simulation shown in Fig. 11b. Although the simulated NO_2 mixing ratios are slightly lower than the observations (Fig. 11c), EMAC captures the overall diurnal variability well.

https://doi.org/10.5194/egusphere-2026-5912
Preprint. Discussion started: 11 November 2026
© Author(s) 2026. CC BY 4.0 License.

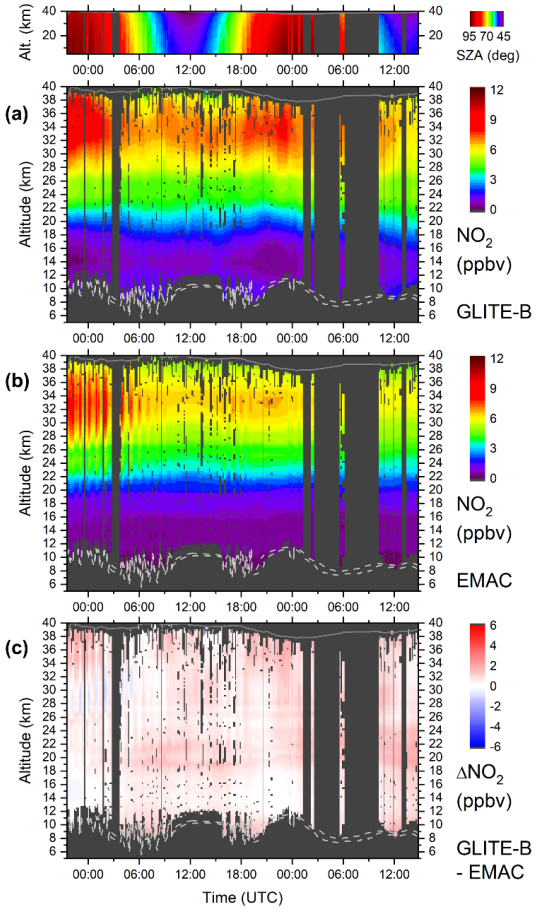


Figure 11. Same as Fig. 10 but for NO_2. The measured data **(a)** have been temporally smoothed using a 39-point adjacent averaging routine to attenuate noisy structures. Consequently, VMR variations caused by azimuthal line-of-sight rotations are strongly smoothed.

460

3.2.2 PAN, HCOOH, and CH_3OH

Peroxyacetyl nitrate (PAN), formic acid (HCOOH), and methanol (CH_3OH) are trace gases associated with pollution and are characterized by different atmospheric lifetimes. PAN is formed by the reaction of NO_2 with the peroxyacetyl radical ($CH_3C(O)O_2$), which is produced
465 during the oxidation of non-methane volatile organic compounds (NMVOCs). In the cold upper troposphere, PAN can persist for several weeks to months (Fischer et al., 2014; Glatthor et al., 2007; Singh, 1987). HCOOH originates from direct emissions, including biogenic sources, biomass burning, and fossil fuel combustion, as well as from secondary photochemical

https://doi.org/10.5194/egusphere-2026-5912
Preprint. Discussion started: 11 November 2026
© Author(s) 2026. CC BY 4.0 License.

production involving anthropogenic and biogenic precursors (Mungall et al., 2018). Its atmospheric lifetime in the free troposphere is on the order of a few weeks (Millet et al., 2015). CH_3OH is emitted primarily by terrestrial vegetation and the oceans, with additional contributions from biomass burning and anthropogenic sources, and is also formed secondarily through the oxidation of volatile organic compounds. Its mean atmospheric lifetime is approximately 5 days (Bates et al., 2021).

Figure 12a shows the PAN distribution in the UTLS measured by GLITE-B along the flight path together with the corresponding EMAC simulation. Enhanced PAN mixing ratios are observed along the dynamical tropopause in both the measurements and the simulation. Mixing ratios of up to 0.6 ppbv are consistent with previous observations in the upper troposphere (e.g. Fischer et al., 2014; Glatthor et al., 2007; Johansson et al., 2022; Wetzel et al., 2021). The EMAC simulation reproduces the observed PAN distribution well, both in terms of its spatial extent and absolute mixing ratios. However, differences are apparent between approximately 18:00 and 00:00 UTC, where EMAC shows PAN filling the troposphere more uniformly, whereas GLITE-B observes a gradual increase in PAN mixing ratios with altitude, broadly following the cloud-edge structure.

In contrast, the temporal distributions of HCOOH (Fig. 12b) and CH_3OH (Fig. 12c) exhibit only limited regions of enhanced mixing ratios, reflecting their shorter atmospheric lifetimes and different source strengths. Maximum mixing ratios of up to 0.25 ppbv for HCOOH and 3.0 ppbv for CH_3OH are consistent with previous observations in the UTLS region (e.g. Glatthor et al., 2013; Johansson et al., 2022). While EMAC reproduces the general location of these enhanced regions, the simulated mixing ratios are substantially lower than the measured ones. The agreement in the location of the enhanced regions, together with the good representation of PAN, suggests that the large-scale transport of polluted air masses is reasonably captured by EMAC. The substantially lower HCOOH and CH_3OH mixing ratios may instead reflect underestimated direct and precursor emissions and/or limitations in the representation of their secondary chemical production and loss.

https://doi.org/10.5194/egusphere-2026-5912
Preprint. Discussion started: 11 November 2026
© Author(s) 2026. CC BY 4.0 License.

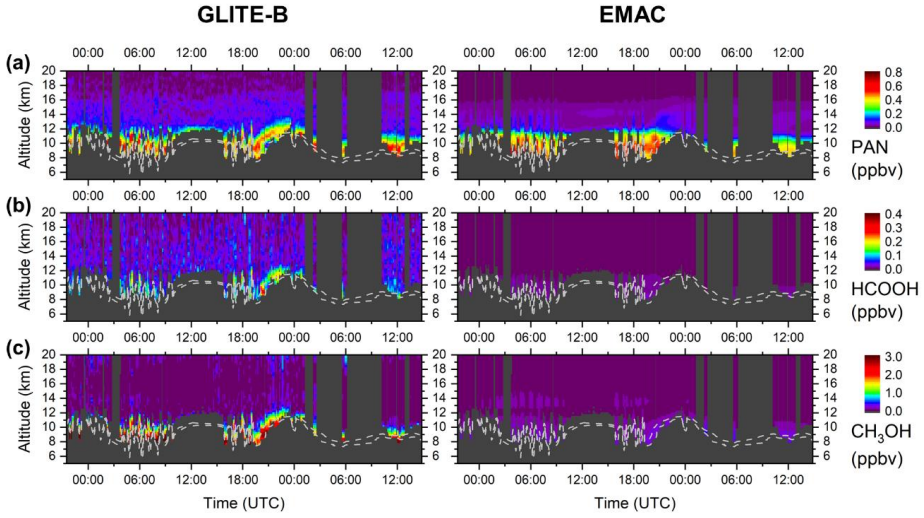


Figure 12. Temporal evolution of PAN **(a)**, HCOOH **(b)**, and CH_3OH **(c)** observed by GLITE-B (left) and simulated by EMAC (right) between 22 and 24 June 2024 in the UTLS above the North Atlantic. The dynamical tropopause using ECMWF 2 and 4 potential vorticity (PV) units is indicated as dashed grey lines.

3.2.3 CFC-11, CFC-12, and SF_6

Trichlorofluoromethane, also called CFC-11 (CCl_3F), and dichlorodifluoromethane, known as CFC-12 (CCl_2F_2), are long-lived chlorofluorocarbons (CFCs) regulated under the Montreal Protocol and are removed from the stratosphere primarily by photolysis (e.g. Ko and Dak Sze, 1982). Following the phase-out of their production and consumption, their tropospheric concentrations have been declining over the past decades (e.g. Prinn et al., 2018). Since the atmospheric lifetime of CFC-12 (approximately 102 years) is about twice that of CFC-11 (Hoffmann et al., 2014), its stratospheric decrease in VMR is less pronounced than that of CFC-11. Figure 13 shows the correlation of CFC-11 and CFC-12. Such a tracer–tracer correlation provides an additional consistency check for the retrievals, as both long-lived species are transported by the same large-scale circulation while exhibiting different stratospheric photochemical lifetimes. The altitude colour-coding of the GLITE-B measurements shows the expected decrease in the volume mixing ratios of both CFCs with altitude. The mean GLITE-B correlation exhibits a gently curved shape with a wave-like feature around 25 km. This feature is related to the dynamical structure previously identified in the measured vertical profiles of O_3, H_2O, and N_2O and is clearly reproduced by the EMAC

https://doi.org/10.5194/egusphere-2026-5912
Preprint. Discussion started: 11 November 2026
© Author(s) 2026. CC BY 4.0 License.

simulation. A mean correlation previously derived from a GLORIA balloon flight launched from Kiruna on 21-22 August 2021 (Wetzel et al., 2025) does not exhibit such a dynamical signature, but the correlation values are within a comparable range to those observed by GLITE-B. Correlation data from cryosampler measurements (Schuck et al., 2025; Wetzel et al., 2025) carried out over Kiruna a few days before the GLORIA-B flight, as well as from an earlier MIPAS balloon observation in July 2003 (Wetzel et al., 2022), are likewise consistent with the retrieved GLITE-B data within the measurement uncertainties. The same applies to the Northern Hemisphere lower-tropospheric reference value from the Advanced Global Atmospheric Gases Experiment (AGAGE) network (Prinn et al., 2018).

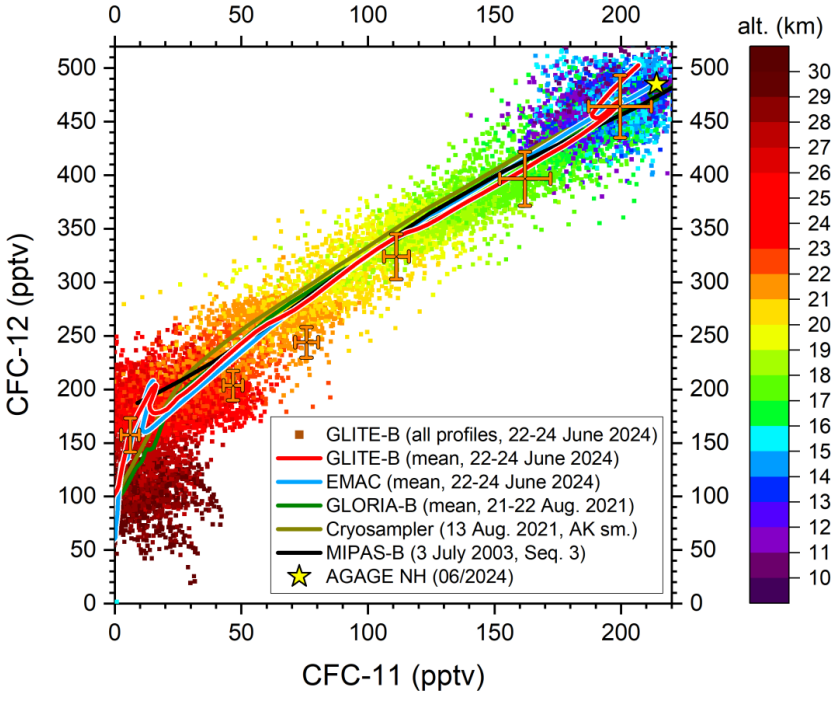


Figure 13. Correlation between the tracer species CFC-11 and CFC-12 measured by GLITE-B on 22-24 June 2024 (altitude-colour-coded squares) up to 30 km altitude. Total error bars (orange) are shown for selected data points. The mean GLITE-B correlation (red line) and the corresponding mean EMAC simulation (blue line) are also displayed. For comparison, the mean GLORIA-B observations from a balloon flight over northern Scandinavia (Kiruna) on 21-22 August 2021 (green line; Wetzel et al., 2025) and cryosampler measurements obtained at the same location on 13 August 2021 (dark yellow line; Schuck et al., 2025; Wetzel et al., 2025) are included. In addition, measurements from an earlier MIPAS balloon flight over northern Scandinavia (black line; Wetzel et al., 2022) are shown. The Northern Hemisphere lower tropospheric reference value from the AGAGE network (yellow star; Prinn et al., 2018) agrees with the GLITE-B measurements in the UTLS region.

https://doi.org/10.5194/egusphere-2026-5912
Preprint. Discussion started: 11 November 2026
© Author(s) 2026. CC BY 4.0 License.

The atmospheric lifetime of sulphur hexafluoride (SF_6) is about a factor of 20 longer than that of CFC-12 because SF_6 is chemically inert in the stratosphere (Vervalcke et al., 2026). Figure 14 compares the measured evolution of SF_6 (Fig. 14a) with the corresponding EMAC simulation (Fig. 14b). The expected decrease with altitude in the stratospheric SF_6 VMR is clearly evident in both the measurements and the EMAC simulation. The dynamical feature near 26 km, as already apparent in the O_3, H_2O and N_2O observations, is also visible in both the measurements and the simulation. Although SF_6 is chemically inert in the stratosphere, its mixing ratio decreases with altitude. This decrease is primarily caused by atmospheric transport, as tropospheric SF_6 abundances continue to rise (Prinn et al., 2018; Simmonds et al., 2020). While the mean age of air increases with altitude, older air masses in the upper stratosphere contain lower SF_6 mixing ratios than younger air in the lower stratosphere (Hall and Plumb, 1994; Hall and Waugh, 1998). In addition, stratospheric SF_6 mixing ratios are influenced by the downward transport of SF_6-depleted air from the mesosphere (Voet et al., 2025). At 10 km, a mean SF_6 mixing ratio of 12 pptv is observed, in excellent agreement with the Northern Hemisphere lower tropospheric value reported by the AGAGE network (Prinn et al., 2018). The EMAC simulation also yields a mean SF_6 mixing ratio of 12 pptv at 10 km. However, the decrease in SF_6 VMR with altitude is somewhat more pronounced in the EMAC simulation than in the GLITE-B measurements above approximately 16 km (Fig. 14c). This discrepancy may be at least partly explained by deficiencies in the simulated transport of air masses and/or by uncertainties in the representation of SF_6 photolysis in the mesosphere.

https://doi.org/10.5194/egusphere-2026-5912
Preprint. Discussion started: 11 November 2026
© Author(s) 2026. CC BY 4.0 License.

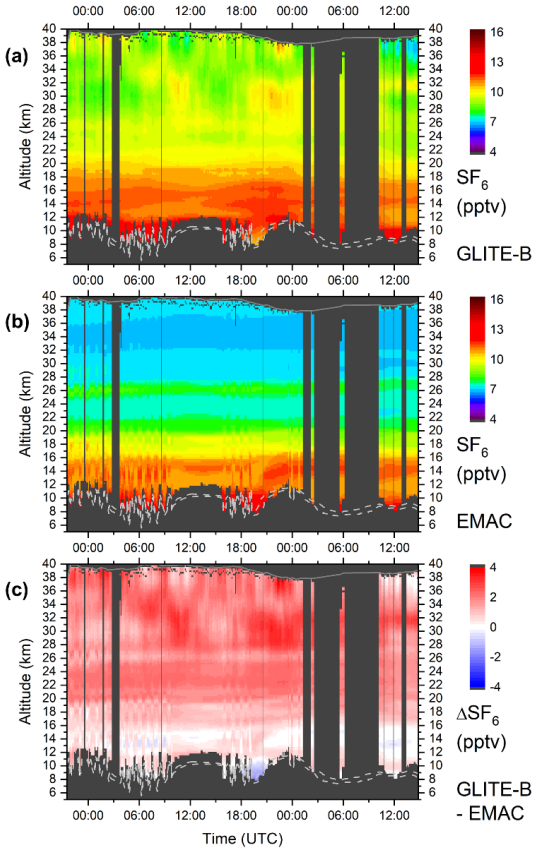


Figure 14. Same as Fig. 10 but for SF_6 (without the solar zenith angle). The measured data **(a)** have been temporally smoothed using a 39-point adjacent averaging filter to suppress noisy structures. As a result, VMR variations caused by azimuthal line-of-sight rotations are no longer apparent.

4 Conclusions

Vertical profiles of a range of trace gases were retrieved from limb-imaging infrared emission spectra measured during the first balloon flight of the new GLITE-B instrument over the North Atlantic. The primary objective of the mission was to demonstrate the technical performance of the new GLITE balloon instrument and its capability to perform reliable long-duration atmospheric observations over several days.

In a first step, temperature, O_3, HNO_3, H_2O, and N_2O were compared with MLS version 6 satellite measurements to assess the quality and reliability of the GLITE-B observations. EMAC model simulations were additionally used as an independent consistency check together with

https://doi.org/10.5194/egusphere-2026-5912
Preprint. Discussion started: 11 November 2026
© Author(s) 2026. CC BY 4.0 License.

ECMWF ERA5 analyses (for temperature, H_2O and O_3). Differences between the mean vertical profiles of temperature and the trace gases O_3, HNO_3, H_2O, and N_2O remained largely within the combined error limits. Over wide altitude regions in the stratosphere differences stayed within ±2 K for temperature and ±10 % for the retrieved gases. In the case of N_2O below 27 km a negative bias of approximately 20 % was found in the MLS data with respect to GLITE-B.

In a second step, photochemically active species ($ClONO_2$, NO_2), pollution trace gases (PAN, HCOOH, CH_3OH), as well as additional long-lived tropospheric source gases were compared to EMAC simulations. The observed diurnal variability of $ClONO_2$ and NO_2 in the sunlit summer polar stratosphere is captured well by EMAC. The pollution gas PAN is also well reproduced by EMAC, while for HCOOH and CH_3OH EMAC captures the general location of measured enhanced regions, but the simulated mixing ratios are substantially lower than the measured ones. This discrepancy may reflect underestimated direct and precursor emissions in EMAC and/or limitations in the representation of the secondary chemical production and loss of HCOOH and CH_3OH. The tracer–tracer relationship between CFC-11 and CFC-12 and the observed SF_6 profiles are consistent with current knowledge of stratospheric transport.

In conclusion, the first long-duration trans-Atlantic balloon flight of the new GLITE-B instrument successfully demonstrated its capability to deliver accurate, high-vertical-resolution profiles of various trace gases within expected uncertainty ranges. The observations show good agreement with independent satellite (MLS) measurements, previous balloon observations, and EMAC simulations over large parts of the UTLS and stratosphere. In addition to the spatial distribution of trace gases, GLITE-B provides unique information on their temporal evolution over several days, enabling investigations of transport and photochemical processes. These results demonstrate the considerable potential of GLITE-B for future long-duration balloon missions to investigate atmospheric composition and chemistry from the upper troposphere to the upper stratosphere. In a broader context, these results further highlight the substantial potential of space-borne infrared limb imaging for monitoring the state and temporal evolution of the UTLS and stratosphere, including their sensitivity to ongoing changes in atmospheric composition and dynamics. Accurate quantification of radiatively active trace gases in the UTLS is essential for assessing their contributions to radiative forcing and climate, as even small changes in this region can have disproportionate effects. Such measurements are particularly important in view of the ongoing decline in observational capabilities (Salawitch et al., 2025), which risks leaving this region increasingly under-observed.

https://doi.org/10.5194/egusphere-2026-5912
Preprint. Discussion started: 11 November 2026
© Author(s) 2026. CC BY 4.0 License.



Data availability. GLITE-B measurements will be available on the KITopen repository. EMAC data are available upon request.

Author contributions. GW wrote most of the manuscript and performed the majority of the data analysis, with input from all co-authors. AK, JU, MH, PP, SJ, and WW were involved in the GLITE-B data processing and scientific discussions throughout the project. CP, EK, FFV, GM, GS, MR, RS, TG, and TN developed and characterized the instrument. OK performed the EMAC simulations. MLS analyzed and interpreted MLS data. BMS, JC, MIH, PB, and VC provided institutional leadership for the project. All authors contributed to the final manuscript.

Competing interests. The authors declare that they have no conflict of interest.

Acknowledgements. We thank the Centre National d'Études Spatiales (CNES) for the excellent balloon operations during the TRANSAT 2024 campaign. This work is based on observations during the first CNES transatlantic flight under a balloon operated and supported by CNES, under the agreement between CNES and CNRS/INSU, within the TRANSAT 2024 campaign. Work at the Jet Propulsion Laboratory, California Institute of Technology, was carried out under a contract with the National Aeronautics and Space Administration (80NM0018D0004). We gratefully acknowledge the computing resources provided by the National High-Performance Computing Center at KIT (NHR@KIT) on the HoreKa high-performance computer, provided by NHR@KIT, supported by the Federal Ministry of Research, Technology and Space and the Ministry of Science, Research and the Arts of Baden-Württemberg through the NHR joint funding program

Financial support. The article processing charges for this open-access publication were covered by the Karlsruhe Institute of Technology (KIT).

https://doi.org/10.5194/egusphere-2026-5912
Preprint. Discussion started: 11 November 2026
© Author(s) 2026. CC BY 4.0 License.

References

Alvarado, L. M. A., Richter, A., Vrekoussis, M., Hilboll, A., Kalisz Hedegaard, A. B., Schneising, O., and Burrows, J. P.: Unexpected long-range transport of glyoxal and formaldehyde observed from the Copernicus Sentinel-5 Precursor satellite during the 2018 Canadian wildfires, Atmos. Chem. Phys., 20, 2057–2072, https://doi.org/10.5194/acp-20-2057-2020, 2020.

Atkinson, R., Baulch, D. L., Cox, R. A., Crowley, J. N., Hampson, R. F., Hynes, R. G., Jenkin, M. E., Rossi, M. J., and Troe, J.: Evaluated kinetic and photochemical data for atmospheric chemistry: Volume III - gas phase reactions of inorganic halogens, Atmos. Chem. Phys., 7, 981–1191, https://doi.org/10.5194/acp-7-981-2007, 2007.

Bates, K. H., Jacob, D. J., Wang, S., Hornbrook, R. S., Apel, E. C., Kim, M. J., Millet, D. B., Wells, K. C., Chen, X., Brewer, J. F., Ray, E. A., Commane, R., Diskin, G. S., and Wofsy, S. C.: The Global Budget of Atmospheric Methanol: New Constraints on Secondary, Oceanic, and Terrestrial Sources, J. Geophys. Res. Atmos., 126, https://doi.org/10.1029/2020JD033439, 2021.

Brasseur, G. P. and Solomon, S.: Aeronomy of the Middle Atmosphere: Chemistry and Physics of the Stratosphere and Mesosphere, Third revised and enlarged edition., Springer, Dordrecht, https://doi.org/10.1007/1-4020-3824-0, 2005.

Brasunas, J. C., Kunde, V. G., and Herath, L. W.: Cryogenic Fourier spectrometer for measuring trace species in the lower stratosphere, Appl. Opt., 27, 4964, https://doi.org/10.1364/AO.27.004964, 1988.

Burkholder, J. B., Sander, S. P., Abbatt, J. P. D., Barker, J. R., Huie, R. E., Kolb, C. E., Kurylo, M. J., Orkin, V. L., Wilmouth, D. M., and Wine, P. H.: Chemical Kinetics and Photochemical Data for Use in Atmospheric Studies, Evaluation no. 18, JPL Publ 15-10 Jet Propuls. Lab. Pasadena CA, 2015.

Carli, B., Mencaraglia, F., and Bonetti, A.: Submillimeter high-resolution FT spectrometer for atmospheric studies, Appl. Opt., 23, 2594, https://doi.org/10.1364/AO.23.002594, 1984.

Chipperfield, M. P. and Bekki, S.: Opinion: Stratospheric ozone – depletion, recovery and new challenges, Atmos. Chem. Phys., 24, 2783–2802, https://doi.org/10.5194/acp-24-2783-2024, 2024.

https://doi.org/10.5194/egusphere-2026-5912
Preprint. Discussion started: 11 November 2026
© Author(s) 2026. CC BY 4.0 License.

von Clarmann, T. and Johansson, S.: Chlorine nitrate in the atmosphere, Atmos. Chem. Phys., 18, 15363–15386, https://doi.org/10.5194/acp-18-15363-2018, 2018.

von Clarmann, T., Fischer, H., Friedl-Vallon, F., Linden, A., Oelhaf, H., Piesch, C., Seefeldner, M., and Völker, W.: Retrieval of stratospheric O_3, HNO_3 and $ClONO_2$ profiles from 1992 MIPAS-B limb emission spectra: Method, results, and error analysis, J. Geophys. Res., 98, 20495, https://doi.org/10.1029/93JD02261, 1993.

von Clarmann, T., Wetzel, G., Oelhaf, H., Friedl-Vallon, F., Linden, A., Maucher, G., Seefeldner, M., Trieschmann, O., and Lefèvre, F.: $ClONO_2$ vertical profile and estimated mixing ratios of ClO and HOCl in winter Arctic stratosphere from Michelson interferometer for passive atmospheric sounding limb emission spectra, J. Geophys. Res., 102, 16157–16168, https://doi.org/10.1029/97JD00605, 1997.

Dessler, A. E., Schoeberl, M. R., Wang, T., Davis, S. M., Rosenlof, K. H., and Vernier, J.-P.: Variations of stratospheric water vapor over the past three decades, J. Geophys. Res. Atmos., 119, 12588–12598, https://doi.org/10.1002/2014JD021712, 2014.

Eyring, V., Bony, S., Meehl, G. A., Senior, C. A., Stevens, B., Stouffer, R. J., and Taylor, K. E.: Overview of the Coupled Model Intercomparison Project Phase 6 (CMIP6) experimental design and organization, Geosci. Model Dev., 9, 1937–1958, https://doi.org/10.5194/gmd-9-1937-2016, 2016.

Fischer, E. V., Jacob, D. J., Yantosca, R. M., Sulprizio, M. P., Millet, D. B., Mao, J., Paulot, F., Singh, H. B., Roiger, A., Ries, L., Talbot, R. W., Dzepina, K., and Pandey Deolal, S.: Atmospheric peroxyacetyl nitrate (PAN): a global budget and source attribution, Atmos. Chem. Phys., 14, 2679–2698, https://doi.org/10.5194/acp-14-2679-2014, 2014.

Fischer, H. and Oelhaf, H.: Remote sensing of vertical profiles of atmospheric trace constituents with MIPAS limb-emission spectrometers, Appl. Opt., 35, 2787–2796, 1996.

Fischer, H., Birk, M., Blom, C., Carli, B., Carlotti, M., von Clarmann, T., Delbouille, L., Dudhia, A., Ehhalt, D., Endemann, M., Flaud, J. M., Gessner, R., Kleinert, A., Koopman, R., Langen, J., López-Puertas, M., Mosner, P., Nett, H., Oelhaf, H., Perron, G., Remedios, J., Ridolfi, M., Stiller, G., and Zander, R.: MIPAS: an instrument for atmospheric and climate research, Atmos. Chem. Phys., 8, 2151–2188, https://doi.org/10.5194/acp-8-2151-2008, 2008.

https://doi.org/10.5194/egusphere-2026-5912
Preprint. Discussion started: 11 November 2026
© Author(s) 2026. CC BY 4.0 License.



Forster, P. M. de F. and Shine, K. P.: Radiative forcing and temperature trends from stratospheric ozone changes, J. Geophys. Res., 102, 10841–10855, https://doi.org/10.1029/96JD03510, 1997.

Forster, P. M. de F. and Shine, K. P.: Assessing the climate impact of trends in stratospheric water vapor, Geophys. Res. Lett., 29, 10-1-10–4, https://doi.org/10.1029/2001GL013909, 2002.

Friedl-Vallon, F., Maucher, G., Seefeldner, M., Trieschmann, O., Kleinert, A., Lengel, A., Keim, C., Oelhaf, H., and Fischer, H.: Design and characterization of the balloon-borne Michelson Interferometer for Passive Atmospheric Sounding (MIPAS-B2), Appl. Opt., 43, 3335, https://doi.org/10.1364/AO.43.003335, 2004.

Friedl-Vallon, F., Gulde, T., Hase, F., Kleinert, A., Kulessa, T., Maucher, G., Neubert, T., Olschewski, F., Piesch, C., Preusse, P., Rongen, H., Sartorius, C., Schneider, H., Schönfeld, A., Tan, V., Bayer, N., Blank, J., Dapp, R., Ebersoldt, A., Fischer, H., Graf, F., Guggenmoser, T., Höpfner, M., Kaufmann, M., Kretschmer, E., Latzko, T., Nordmeyer, H., Oelhaf, H., Orphal, J., Riese, M., Schardt, G., Schillings, J., Sha, M. K., Suminska-Ebersoldt, O., and Ungermann, J.: Instrument concept of the imaging Fourier transform spectrometer GLORIA, Atmos. Meas. Tech., 7, 3565–3577, https://doi.org/10.5194/amt-7-3565-2014, 2014.

Gettelman, A., Hoor, P., Pan, L. L., Randel, W. J., Hegglin, M. I., and Birner, T.: The extratropical upper troposphere and lower stratosphere, Rev. Geophys., 49, 555, https://doi.org/10.1029/2011RG000355, 2011.

Glatthor, N., Clarmann, T., Fischer, H., Funke, B., Grabowski, U., Höpfner, M., Kellmann, S., Kiefer, M., Linden, A., Milz, M., Steck, T., and Stiller, G. P.: Global peroxyacetyl nitrate (PAN) retrieval in the upper troposphere from limb emission spectra of the Michelson Interferometer for Passive Atmospheric Sounding (MIPAS), Atmos. Chem. Phys., 7, 2775–2787, https://doi.org/10.5194/acp-7-2775-2007, 2007.

Glatthor, N., Höpfner, M., Semeniuk, K., Lupu, A., Palmer, P. I., McConnell, J. C., Kaminski, J. W., Clarmann, T., Stiller, G. P., Funke, B., Kellmann, S., Linden, A., and Wiegele, A.: The Australian bushfires of February 2009: MIPAS observations and GEM-AQ model results, Atmos. Chem. Phys., 13, 1637–1658, https://doi.org/10.5194/acp-13-1637-2013, 2013.

Gordon, I. E., Rothman, L. S., Hill, C., Kochanov, R. V., Tan, Y., Bernath, P. F., Birk, M., Boudon, V., Campargue, A., Chance, K. V., Drouin, B. J., Flaud, J.-M., Gamache, R. R.,

https://doi.org/10.5194/egusphere-2026-5912
Preprint. Discussion started: 11 November 2026
© Author(s) 2026. CC BY 4.0 License.

Hodges, J. T., Jacquemart, D., Perevalov, V. I., Perrin, A., Shine, K. P., Smith, M.-A. H., Tennyson, J., Toon, G. C., Tran, H., Tyuterev, V. G., Barbe, A., Császár, A. G., Devi, V. M., Furtenbacher, T., Harrison, J. J., Hartmann, J.-M., Jolly, A., Johnson, T. J., Karman, T., Kleiner, I., Kyuberis, A. A., Loos, J., Lyulin, O. M., Massie, S. T., Mikhailenko, S. N., Moazzen-Ahmadi, N., Müller, H. S. P., Naumenko, O. V., Nikitin, A. V., Polyansky, O. L., Rey, M., Rotger, M., Sharpe, S. W., Sung, K., Starikova, E., Tashkun, S. A., Auwera, J. V., Wagner, G., Wilzewski, J., Wcisło, P., Yu, S., and Zak, E. J.: The HITRAN2016 molecular spectroscopic database, J. Quant. Spectrosc. Radiat. Transf., 203, 3–69, https://doi.org/10.1016/j.jqsrt.2017.06.038, 2017.

Gordon, I. E., Rothman, L. S., Hargreaves, R. J., Hashemi, R., Karlovets, E. V., Skinner, F. M., Conway, E. K., Hill, C., Kochanov, R. V., Tan, Y., Wcisło, P., Finenko, A. A., Nelson, K., Bernath, P. F., Birk, M., Boudon, V., Campargue, A., Chance, K. V., Coustenis, A., Drouin, B. J., Flaud, J. –M., Gamache, R. R., Hodges, J. T., Jacquemart, D., Mlawer, E. J., Nikitin, A. V., Perevalov, V. I., Rotger, M., Tennyson, J., Toon, G. C., Tran, H., Tyuterev, V. G., Adkins, E. M., Baker, A., Barbe, A., Canè, E., Császár, A. G., Dudaryonok, A., Egorov, O., Fleisher, A. J., Fleurbaey, H., Foltynowicz, A., Furtenbacher, T., Harrison, J. J., Hartmann, J. –M., Horneman, V. –M., Huang, X., Karman, T., Karns, J., Kassi, S., Kleiner, I., Kofman, V., Kwabia–Tchana, F., Lavrentieva, N. N., Lee, T. J., Long, D. A., Lukashevskaya, A. A., Lyulin, O. M., Makhnev, V. Yu., Matt, W., Massie, S. T., Melosso, M., Mikhailenko, S. N., Mondelain, D., Müller, H. S. P., Naumenko, O. V., Perrin, A., Polyansky, O. L., Raddaoui, E., Raston, P. L., Reed, Z. D., Rey, M., Richard, C., Tóbiás, R., Sadiek, I., Schwenke, D. W., Starikova, E., Sung, K., Tamassia, F., Tashkun, S. A., Vander Auwera, J., Vasilenko, I. A., Vigasin, A. A., Villanueva, G. L., Vispoel, B., Wagner, G., Yachmenev, A., and Yurchenko, S. N.: The HITRAN2020 molecular spectroscopic database, J. Quant. Spectrosc. Radiat. Transf., 277, 107949, https://doi.org/10.1016/j.jqsrt.2021.107949, 2022.

Gordon, I. E., Rothman, L. S., Hargreaves, R. J., Gomez, F. M., Bertin, T., Hill, C., Kochanov, R. V., Tan, Y., Wcisło, P., Makhnev, V. Yu., Bernath, P. F., Birk, M., Boudon, V., Campargue, A., Coustenis, A., Drouin, B. J., Gamache, R. R., Hodges, J. T., Jacquemart, D., Mlawer, E. J., Nikitin, A. V., Perevalov, V. I., Rotger, M., Robert, S., Tennyson, J., Toon, G. C., Tran, H., Tyuterev, V. G., Adkins, E. M., Barbe, A., Bailey, D. M., Bielska, K., Bizzocchi, L., Blake, T. A., Bowesman, C. A., Cacciani, P., Čermák, P., Császár, A. G., Denis, L., Egbert, S. C., Egorov, O., Ermilov, A. Yu., Fleisher, A. J., Fleurbaey, H., Foltynowicz, A., Furtenbacher, T., Germann,

https://doi.org/10.5194/egusphere-2026-5912
Preprint. Discussion started: 11 November 2026
© Author(s) 2026. CC BY 4.0 License.



M., Guest, E. R., Harrison, J. J., Hartmann, J.-M., Hjältén, A., Hu, S.-M., Huang, X., Johnson, T. J., Jóźwiak, H., Kassi, S., Khan, M. V., Kwabia-Tchana, F., Lee, T. J., Lisak, D., Liu, A.-W., Lyulin, O. M., Malarich, N. A., Manceron, L., Marinina, A. A., Massie, S. T., Mascio, J., Medvedev, E. S., Meshkov, V. V., Mellau, G. Ch., Melosso, M., Mikhailenko, S. N., Mondelain, D., Müller, H. S. P., O'Donnell, M., Owens, A., Perrin, A., Polyansky, O. L., Raston, P. L., Reed, Z. D., Rey, M., Richard, C., Rieker, G. B., Röske, C., Sharpe, S. W., Starikova, E., Stolarczyk, N., Stolyarov, A. V., Sung, K., Tamassia, F., Terragni, J., Ushakov, V. G., Vasilchenko, S., Vispoel, B., Vodopyanov, K. L., Wagner, G., Wójtewicz, S., Yurchenko, S. N., and Zobov, N. F.: The HITRAN2024 molecular spectroscopic database, J. Quant. Spectrosc. Radiat. Transf., 353, 109807, https://doi.org/10.1016/j.jqsrt.2026.109807, 2026.

Hall, T. M. and Plumb, R. A.: Age as a diagnostic of stratospheric transport, J. Geophys. Res. Atmos., 99, 1059–1070, https://doi.org/10.1029/93JD03192, 1994.

Hall, T. M. and Waugh, D. W.: Influence of nonlocal chemistry on tracer distributions: Inferring the mean age of air from SF_6, J. Geophys. Res. Atmos., 103, 13327–13336, https://doi.org/10.1029/98JD00170, 1998.

Hansen, J., Sato, M., and Ruedy, R.: Radiative forcing and climate response, J. Geophys. Res. Atmos., 102, 6831–6864, https://doi.org/10.1029/96JD03436, 1997.

Hersbach, H., Bell, B., Berrisford, P., Hirahara, S., Horányi, A., Muñoz-Sabater, J., Nicolas, J., Peubey, C., Radu, R., Schepers, D., Simmons, A., Soci, C., Abdalla, S., Abellan, X., Balsamo, G., Bechtold, P., Biavati, G., Bidlot, J., Bonavita, M., De Chiara, G., Dahlgren, P., Dee, D., Diamantakis, M., Dragani, R., Flemming, J., Forbes, R., Fuentes, M., Geer, A., Haimberger, L., Healy, S., Hogan, R. J., Hólm, E., Janisková, M., Keeley, S., Laloyaux, P., Lopez, P., Lupu, C., Radnoti, G., De Rosnay, P., Rozum, I., Vamborg, F., Villaume, S., and Thépaut, J.: The ERA5 global reanalysis, Q. J. R. Meteorol. Soc., 146, 1999–2049, https://doi.org/10.1002/qj.3803, 2020.

Hoffmann, L., Hoppe, C. M., Müller, R., Dutton, G. S., Gille, J. C., Griessbach, S., Jones, A., Meyer, C. I., Spang, R., Volk, C. M., and Walker, K. A.: Stratospheric lifetime ratio of CFC-11 and CFC-12 from satellite and model climatologies, Atmos. Chem. Phys., 14, 12479–12497, https://doi.org/10.5194/acp-14-12479-2014, 2014.

https://doi.org/10.5194/egusphere-2026-5912
Preprint. Discussion started: 11 November 2026
© Author(s) 2026. CC BY 4.0 License.



Höpfner, M., Oelhaf, H., Wetzel, G., Friedl-Vallon, F., Kleinert, A., Lengel, A., Maucher, G., Nordmeyer, H., Glatthor, N., Stiller, G., von Clarmann, T., Fischer, H., Kröger, C., and Deshler, T.: Evidence of scattering of tropospheric radiation by PSCs in mid-IR limb emission spectra: MIPAS-B observations and KOPRA simulations, Geophys. Res. Lett., 29, 119-1-119–4, https://doi.org/10.1029/2001GL014443, 2002.

Jöckel, P., Kerkweg, A., Pozzer, A., Sander, R., Tost, H., Riede, H., Baumgaertner, A., Gromov, S., and Kern, B.: Development cycle 2 of the Modular Earth Submodel System (MESSy2), Geosci. Model Dev., 3, 717–752, https://doi.org/10.5194/gmd-3-717-2010, 2010.

Johansson, S., Wetzel, G., Friedl-Vallon, F., Glatthor, N., Höpfner, M., Kleinert, A., Neubert, T., Sinnhuber, B.-M., and Ungermann, J.: Biomass burning pollution in the South Atlantic upper troposphere: GLORIA trace gas observations and evaluation of the CAMS model, Atmos. Chem. Phys., 22, 3675–3691, https://doi.org/10.5194/acp-22-3675-2022, 2022.

Johnson, D. G., Jucks, K. W., Traub, W. A., and Chance, K. V.: Smithsonian stratospheric far-infrared spectrometer and data reduction system, J Geophys Res, 100, 3091–3106, https://doi.org/10.1029/94JD02685, 1995.

Khosrawi, F., Lossow, S., Stiller, G. P., Rosenlof, K. H., Urban, J., Burrows, J. P., Damadeo, R. P., Eriksson, P., García-Comas, M., Gille, J. C., Kasai, Y., Kiefer, M., Nedoluha, G. E., Noël, S., Raspollini, P., Read, W. G., Rozanov, A., Sioris, C. E., Walker, K. A., and Weigel, K.: The SPARC water vapour assessment II: comparison of stratospheric and lower mesospheric water vapour time series observed from satellites, Atmos. Meas. Tech., 11, 4435–4463, https://doi.org/10.5194/amt-11-4435-2018, 2018.

Ko, M. K. W. and Dak Sze, N.: A 2-D model calculation of atmospheric lifetimes for N_2O, CFC-11 and CFC-12, Nature, 297, 317–319, https://doi.org/10.1038/297317a0, 1982.

Lambert, A., Livesey, N., and Read, W.: MLS/Aura Level 2 Nitrous Oxide (N_2O) Mixing Ratio V006, https://doi.org/10.5067/AURA/MLS/DATA2615, 2026a.

Lambert, A., Read, W., and Livesey, N.: MLS/Aura Level 2 Water Vapor (H_2O) Mixing Ratio V006, https://doi.org/10.5067/AURA/MLS/DATA2608, 2026b.

Livesey, N. J., Read, W. G., Wagner, P. A., Santee, M. L., Froidevaux, L., Schwartz, M. J., Lambert, A., Millán, L. F., Werner, F., Pumphrey, H. C., Manney, G. L., Fuller, R. A., Jarnot, R. F., Knosp, B. W., and Vuu, C.: Version 6.0x Level-2 and Level-3 data quality and description document, https://doi.org/10.5067/AURA/MLS/DOC/v6_dataqualitydocument, 2026.

https://doi.org/10.5194/egusphere-2026-5912
Preprint. Discussion started: 11 November 2026
© Author(s) 2026. CC BY 4.0 License.

Lossow, S., Hurst, D. F., Rosenlof, K. H., Stiller, G. P., Clarmann, T., Brinkop, S., Dameris, M., Jöckel, P., Kinnison, D. E., Plieninger, J., Plummer, D. A., Ploeger, F., Read, W. G., Remsberg, E. E., Russell, J. M., and Tao, M.: Trend differences in lower stratospheric water vapour between Boulder and the zonal mean and their role in understanding fundamental observational discrepancies, Atmos. Chem. Phys., 18, 8331–8351, https://doi.org/10.5194/acp-18-8331-2018, 2018.

Lu, X., Zhang, L., and Shen, L.: Meteorology and Climate Influences on Tropospheric Ozone: a Review of Natural Sources, Chemistry, and Transport Patterns, Curr. Pollut. Rep., 5, 238–260, https://doi.org/10.1007/S40726-019-00118-3, 2019.

Manney, G., Santee, M., Froidevaux, L., Livesey, N., and Read, W.: MLS/Aura Level 2 Nitric Acid (HNO_3) Mixing Ratio V006, https://doi.org/10.5067/AURA/MLS/DATA2611, 2026.

Millán, L., Read, W. G., Santee, M. L., Lambert, A., Manney, G. L., Neu, J. L., Pitts, M. C., Werner, F., Livesey, N. J., and Schwartz, M. J.: The Evolution of the Hunga Hydration in a Moistening Stratosphere, Geophys. Res. Lett., 51, e2024GL110841, https://doi.org/10.1029/2024GL110841, 2024.

Millet, D. B., Baasandorj, M., Farmer, D. K., Thornton, J. A., Baumann, K., Brophy, P., Chaliyakunnel, S., Gouw, J. A., Graus, M., Hu, L., Koss, A., Lee, B. H., Lopez-Hilfiker, F. D., Neuman, J. A., Paulot, F., Peischl, J., Pollack, I. B., Ryerson, T. B., Warneke, C., Williams, B. J., and Xu, J.: A large and ubiquitous source of atmospheric formic acid, Atmos. Chem. Phys., 15, 6283–6304, https://doi.org/10.5194/acp-15-6283-2015, 2015.

Mungall, E. L., Abbatt, J. P. D., Wentzell, J. J. B., Wentworth, G. R., Murphy, J. G., Kunkel, D., Gute, E., Tarasick, D. W., Sharma, S., Cox, C. J., Uttal, T., and Liggio, J.: High gas-phase mixing ratios of formic and acetic acid in the High Arctic, Atmos. Chem. Phys., 18, 10237–10254, https://doi.org/10.5194/acp-18-10237-2018, 2018.

Murcray, F., H., Murcray, F., J., and Murcray, D., G.: Liquid nitrogen-cooled Fourier Transform Spectrometer system for measuring atmospheric emission at high altitudes, J Atmos Ocean Technol, 1, 351–357, 1984.

Nocedal, J. and Wright, S., J.: Numerical optimization, 2nd ed., Springer, New York, https://doi.org/10.1007/978-0-387-40065-5, 2006.

Norton, R. H. and Beer, R.: New apodizing functions for Fourier spectrometry, J. Opt. Soc. Am., 66, 259, https://doi.org/10.1364/JOSA.66.000259, 1976.

https://doi.org/10.5194/egusphere-2026-5912
Preprint. Discussion started: 11 November 2026
© Author(s) 2026. CC BY 4.0 License.



Norton, R. H. and Beer, R.: Errata: New Apodizing Functions For Fourier Spectrometry, J. Opt. Soc. Am., 67, 419, https://doi.org/10.1364/JOSA.67.000419, 1977.

Oelhaf, H., von Clarmann, T., Fischer, H., Friedl-Vallon, F., Fritzsche, Ch., Linden, A., Piesch, Ch., Seefeldner, M., and Völker, W.: Stratospheric $ClONO_2$ and HNO_3 profiles insidethe Arctic vortex from MIPAS-B limb emissionspectra obtained during EASOE, Geophys. Res. Lett., 21, 1263–1266, 1994.

Phillips, D. L.: A technique for the numerical solution of certain integral equations of the first kind, J Assoc Comput Math, 9, 84–97, https://doi.org/10.1145/321105.321114, 1962.

Potapov, P., Tyukavina, A., Turubanova, S., Hansen, M. C., Giglio, L., Hernandez-Serna, A., Lima, A., Harris, N., and Stolle, F.: Unprecedentedly high global forest disturbance due to fire in 2023 and 2024, Proc. Natl. Acad. Sci., 122, e2505418122, https://doi.org/10.1073/pnas.2505418122, 2025.

Prinn, R. G., Weiss, R. F., Arduini, J., Arnold, T., DeWitt, H. L., Fraser, P. J., Ganesan, A. L., Gasore, J., Harth, C. M., Hermansen, O., Kim, J., Krummel, P. B., Li, S., Loh, Z. M., Lunder, C. R., Maione, M., Manning, A. J., Miller, B. R., Mitrevski, B., Mühle, J., O'Doherty, S., Park, S., Reimann, S., Rigby, M., Saito, T., Salameh, P. K., Schmidt, R., Simmonds, P. G., Steele, L. P., Vollmer, M. K., Wang, R. H., Yao, B., Yokouchi, Y., Young, D., and Zhou, L.: History of chemically and radiatively important atmospheric gases from the Advanced Global Atmospheric Gases Experiment (AGAGE), Earth Syst. Sci. Data, 10, 985–1018, https://doi.org/10.5194/essd-10-985-2018, 2018.

Remedios, J. J., Leigh, R. J., Waterfall, A. M., Moore, D. P., Sembhi, H., Parkes, I., Greenhough, J., Chipperfield, M. P., and Hauglustaine, D.: MIPAS reference atmospheres and comparisons to V4.61/V4.62 MIPAS level 2 geophysical data sets, Atmos. Chem. Phys. Discuss., 7, 9973–10017, https://doi.org/10.5194/acpd-7-9973-2007, 2007.

Renard, J.-B., Berthet, G., Brogniez, C., Catoire, V., Fussen, D., Goutail, F., Oelhaf, H., Pommereau, J.-P., Roscoe, H. K., Wetzel, G., Chartier, M., Robert, C., Balois, J.-Y., Verwaerde, C., Auriol, F., François, P., Gaubicher, B., and Wursteisen, P.: Validation of GOMOS-Envisat vertical profiles of O_3, NO_2, NO_3, and aerosol extinction using balloon-borne instruments and analysis of the retrievals, J. Geophys. Res. Space Phys., 113, https://doi.org/10.1029/2007JA012345, 2008.

https://doi.org/10.5194/egusphere-2026-5912
Preprint. Discussion started: 11 November 2026
© Author(s) 2026. CC BY 4.0 License.



Riese, M., Ploeger, F., Rap, A., Vogel, B., Konopka, P., Dameris, M., and Forster, P.: Impact of uncertainties in atmospheric mixing on simulated UTLS composition and related radiative effects, J. Geophys. Res. Atmos., 117, 16305, https://doi.org/10.1029/2012JD017751, 2012.

Riese, M., Oelhaf, H., Preusse, P., Blank, J., Ern, M., Friedl-Vallon, F., Fischer, H., Guggenmoser, T., Höpfner, M., Hoor, P., Kaufmann, M., Orphal, J., Plöger, F., Spang, R., Suminska-Ebersoldt, O., Ungermann, J., Vogel, B., and Woiwode, W.: Gimballed Limb Observer for Radiance Imaging of the Atmosphere (GLORIA) scientific objectives, Atmos. Meas. Tech., 7, 1915–1928, https://doi.org/10.5194/amt-7-1915-2014, 2014.

Roeckner, E., Brokopf, R., Esch, M., Giorgetta, M., Hagemann, S., Kornblueh, L., Manzini, E., Schlese, U., and Schulzweida, U.: Sensitivity of Simulated Climate to Horizontal and Vertical Resolution in the ECHAM5 Atmosphere Model, J. Clim., 19, 3771–3791, https://doi.org/10.1175/JCLI3824.1, 2006.

Sagawa, H., Sato, T. O., Baron, P., Dupuy, E., Livesey, N., Urban, J., von Clarmann, T., Lange, A., Wetzel, G., Connor, B. J., Kagawa, A., Murtagh, D., and Kasai, Y.: Comparison of SMILES ClO profiles with satellite, balloon-borne and ground-based measurements, Atmos. Meas. Tech., 6, 3325–3347, https://doi.org/10.5194/amt-6-3325-2013, 2013.

Salawitch, R. J., Smith, J. B., Selkirk, H., Wargan, K., Chipperfield, M. P., Hossaini, R., Levelt, P. F., Livesey, N. J., McBride, L. A., Millán, L. F., Moyer, E., Santee, M. L., Schoeberl, M. R., Solomon, S., Stone, K., and Worden, H. M.: The Imminent Data Desert: The Future of Stratospheric Monitoring in a Rapidly Changing World, Bull. Am. Meteorol. Soc., 106, E540–E563, https://doi.org/10.1175/BAMS-D-23-0281.1, 2025.

Sander, S. P., Friedl, R. R., Barker, J. R., Golden, D. M., Kurylo, M. J., Wine, P. H., Abbatt, J. P. D., Burkholder, J. B., Kolb, C. E., Moortgat, G. K., Huie, R. E., and Orkin, V. L.: Chemical kinetics and photochemical data for use in atmospheric studies, Evaluation no. 17, JPL Publ 10-6 Jet Propuls. Lab. Pasadena CA, 2011.

Santee, M. L., Manney, G. L., Livesey, N. J., Froidevaux, L., Schwartz, M. J., and Read, W. G.: Trace gas evolution in the lowermost stratosphere from Aura Microwave Limb Sounder measurements, J. Geophys. Res., 116, D18306, https://doi.org/10.1029/2011JD015590, 2011.

Schuck, T. J., Degen, J., Keber, T., Meixner, K., Wagenhäuser, T., Ghysels, M., Durry, G., Amarouche, N., Zanchetta, A., Van Heuven, S., Chen, H., Laube, J. C., Baartman, S., Van Der Veen, C., Popa, M. E., and Engel, A.: Measurement report: Greenhouse gas profiles and age of

https://doi.org/10.5194/egusphere-2026-5912
Preprint. Discussion started: 11 November 2026
© Author(s) 2026. CC BY 4.0 License.



air from the 2021 HEMERA-TWIN balloon launch, Atmos. Chem. Phys., 25, 4333–4348, https://doi.org/10.5194/acp-25-4333-2025, 2025.

Schwartz, M., Froidevaux, L., Livesey, N., and Read, W.: MLS/Aura Level 2 Ozone (O_3) Mixing Ratio V006, https://doi.org/10.5067/AURA/MLS/DATA2616, 2026a.

Schwartz, M., Livesey, N., and Read, W.: MLS/Aura Level 2 Temperature V006, https://doi.org/10.5067/AURA/MLS/DATA2620, 2026b.

Simmonds, P. G., Rigby, M., Manning, A. J., Park, S., Stanley, K. M., McCulloch, A., Henne, S., Graziosi, F., Maione, M., Arduini, J., Reimann, S., Vollmer, M. K., Mühle, J., O'Doherty, S., Young, D., Krummel, P. B., Fraser, P. J., Weiss, R. F., Salameh, P. K., Harth, C. M., Park, M.-K., Park, H., Arnold, T., Rennick, C., Steele, L. P., Mitrevski, B., Wang, R. H. J., and Prinn, R. G.: The increasing atmospheric burden of the greenhouse gas sulfur hexafluoride (SF_6), Atmos. Chem. Phys., 20, 7271–7290, https://doi.org/10.5194/acp-20-7271-2020, 2020.

Singh, H. B.: Reactive nitrogen in the troposphere, Environ. Sci. Technol., 21, 320–7, https://doi.org/10.1021/es00158a001, 1987.

Solomon, S., Rosenlof, K. H., Portmann, R. W., Daniel, J. S., Davis, S. M., Sanford, T. J., and Plattner, G.-K.: Contributions of stratospheric water vapor to decadal changes in the rate of global warming, Science, 327, 1219–23, https://doi.org/10.1126/science.1182488, 2010.

Spang, R., Remedios, J. J., and Barkley, M. P.: Colour indices for the detection and differentiation of cloud types in infra-red limb emission spectra, Adv. Space Res., 33, 1041–1047, https://doi.org/10.1016/S0273-1177(03)00585-4, 2004.

Stiller, G. P., von Clarmann, T., Funke, B., Glatthor, N., Hase, F., Höpfner, M., and Linden, A.: Sensitivity of trace gas abundances retrievals from infrared limb emission spectra to simplifying approximations in radiative transfer modelling, J. Quant. Spectrosc. Radiat. Transf., 72, 249–280, https://doi.org/10.1016/S0022-4073(01)00123-6, 2002.

Stowasser, M., Oelhaf, H., Wetzel, G., Friedl-Vallon, F., Maucher, G., Seefeldner, M., Trieschmann, O., von Clarmann, T., and Fischer, H.: Simultaneous measurements of HDO, H_2O, and CH_4 with MIPAS-B: Hydrogen budget and indication of dehydration inside the polar vortex, J. Geophys. Res., 104, 19213–19225, https://doi.org/10.1029/1999JD900239, 1999.

Stowasser, M., Oelhaf, H., Ruhnke, R., Wetzel, G., Friedl-Vallon, F., Kleinert, A., Kouker, W., Lengel, A., Maucher, G., Nordmeyer, H., Reddmann, Th., Trieschmann, O., von Clarmann, T.,

https://doi.org/10.5194/egusphere-2026-5912
Preprint. Discussion started: 11 November 2026
© Author(s) 2026. CC BY 4.0 License.



Fischer, H., and Chipperfield, M. P.: A characterization of the warm 1999 Arctic winter by observations and modeling: NO_y partitioning and dynamics, J. Geophys. Res., 107, 18861, https://doi.org/10.1029/2001JD001217, 2002.

Stowasser, M., Oelhaf, H., Ruhnke, R., Kleinert, A., Wetzel, G., Friedl-Vallon, F., Kouker, W., Lengel, A., Maucher, G., Nordmeyer, H., Reddmann, Th., and Fischer, H.: The variation of short-lived NO_y species around sunrise at mid-latitudes as measured by MIPAS-B and calculated by KASIMA, Geophys. Res. Lett., 30, 24283, https://doi.org/10.1029/2002GL016727, 2003.

Tikhonov, A. N.: On the solution of ill-posed problems and the method of regularization, Dokl Acad Nauk SSSR, 151, 501–504, 1963.

Ungermann, J., Kleinert, A., Maucher, G., Bartolomé, I., Friedl-Vallon, F., Johansson, S., Krasauskas, L., and Neubert, T.: Quantification and mitigation of the instrument effects and uncertainties of the airborne limb imaging FTIR GLORIA, Atmos. Meas. Tech., 15, 2503–2530, https://doi.org/10.5194/amt-15-2503-2022, 2022.

Vervalcke, S., Errera, Q., Eichinger, R., Reddmann, T., Chabrillat, S., Op De Beeck, M., Stiller, G., and Mahieu, E.: Atmospheric lifetime of sulphur hexafluoride (SF_6) and five other trace gases in the BASCOE model driven by three reanalyses, Atmos. Chem. Phys., 26, 391–409, https://doi.org/10.5194/acp-26-391-2026, 2026.

Voet, F., Ploeger, F., Laube, J., Preusse, P., Konopka, P., Grooß, J.-U., Ungermann, J., Sinnhuber, B.-M., Höpfner, M., Funke, B., Wetzel, G., Johansson, S., Stiller, G., Ray, E., and Hegglin, M. I.: On the estimation of stratospheric age of air from correlations of multiple trace gases, Atmos. Chem. Phys., 25, 3541–3565, https://doi.org/10.5194/acp-25-3541-2025, 2025.

Waibel, A. E., Peter, Th., Carslaw, K. S., Oelhaf, H., Wetzel, G., Crutzen, P. J., Pöschl, U., Tsias, A., Reimer, E., and Fischer, H.: Arctic ozone loss due to denitrification, Science, 283, 2064–2069, https://doi.org/10.1126/science.283.5410.2064, 1999.

Waters, J. W., Froidevaux, L., Harwood, R. S., Jarnot, R. F., Pickett, H. M., Read, W. G., Siegel, P. H., Cofield, R. E., Filipiak, M. J., Flower, D. A., Holden, J. R., Lau, G. K., Livesey, N. J., Manney, G. L., Pumphrey, H. C., Santee, M. L., Wu, D. L., Cuddy, D. T., Lay, R. R., Loo, M. S., Perun, V. S., Schwartz, M. J., Stek, P. C., Thurstans, R. P., Boyles, M. A., Chandra, K. M., Chavez, M. C., Gun-Shing Chen, Chudasama, B. V., Dodge, R., Fuller, R. A., Girard, M. A., Jiang, J. H., Yibo Jiang, Knosp, B. W., LaBelle, R. C., Lam, J. C., Lee, K. A., Miller, D.,

https://doi.org/10.5194/egusphere-2026-5912
Preprint. Discussion started: 11 November 2026
© Author(s) 2026. CC BY 4.0 License.



Oswald, J. E., Patel, N. C., Pukala, D. M., Quintero, O., Scaff, D. M., Van Snyder, W., Tope, M. C., Wagner, P. A., and Walch, M. J.: The Earth observing system microwave limb sounder (EOS MLS) on the aura Satellite, IEEE Trans. Geosci. Remote Sens., 44, 1075–1092, https://doi.org/10.1109/TGRS.2006.873771, 2006.

Waugh, D. and Hall, T. M.: Age of stratospheric air: Theory, observations, and models, Rev. Geophys., 40, 4483, https://doi.org/10.1029/2000RG000101, 2002.

Wetzel, G., von Clarmann, T., Oelhaf, H., and Fischer, H.: Vertical profiles of N_2O_5 along with CH_4, N_2O, and H_2O in the late Arctic winter retrieved from MIPAS-B infrared limb emission measurements, J. Geophys. Res., 100, 23173, https://doi.org/10.1029/95JD02344, 1995.

Wetzel, G., Oelhaf, H., von Clarmann, T., Fischer, H., Friedl-Vallon, F., Maucher, G., Seefeldner, M., Trieschmann, O., and Lefèvre, F.: Vertical profiles of N_2O_5, HO_2NO_2, and NO_2 inside the Arctic vortex, retrieved from nocturnal MIPAS-B2 infrared limb emission measurements in February 1995, J. Geophys. Res., 102, 19177–19186, https://doi.org/10.1029/97JD01311, 1997.

Wetzel, G., Oelhaf, H., Ruhnke, R., Friedl-Vallon, F., Kleinert, A., Kouker, W., Maucher, G., Reddmann, T., Seefeldner, M., Stowasser, M., Trieschmann, O., von Clarmann, T., and Fischer, H.: NO_y partitioning and budget and its correlation with N_2O in the Arctic vortex and in summer midlatitudes in 1997, J. Geophys. Res., 107, 1659, https://doi.org/10.1029/2001JD000916, 2002.

Wetzel, G., Oelhaf, H., Friedl-Vallon, F., Kleinert, A., Lengel, A., Maucher, G., Nordmeyer, H., Ruhnke, R., Nakajima, H., Sasano, Y., Sugita, T., and Yokota, T.: Intercomparison and validation of ILAS-II version 1.4 target parameters with MIPAS-B measurements, J. Geophys. Res., 111, 281, https://doi.org/10.1029/2005JD006287, 2006.

Wetzel, G., Oelhaf, H., Kirner, O., Ruhnke, R., Friedl-Vallon, F., Kleinert, A., Maucher, G., Fischer, H., Birk, M., Wagner, G., and Engel, A.: First remote sensing measurements of ClOOCl along with ClO and $ClONO_2$ in activated and deactivated Arctic vortex conditions using new ClOOCl IR absorption cross sections, Atmos. Chem. Phys., 10, 931–945, https://doi.org/10.5194/acp-10-931-2010, 2010.

Wetzel, G., Oelhaf, H., Kirner, O., Friedl-Vallon, F., Ruhnke, R., Ebersoldt, A., Kleinert, A., Maucher, G., Nordmeyer, H., and Orphal, J.: Diurnal variations of reactive chlorine and

https://doi.org/10.5194/egusphere-2026-5912
Preprint. Discussion started: 11 November 2026
© Author(s) 2026. CC BY 4.0 License.



nitrogen oxides observed by MIPAS-B inside the January 2010 Arctic vortex, Atmos. Chem. Phys., 12, 6581–6592, https://doi.org/10.5194/acp-12-6581-2012, 2012.

Wetzel, G., Oelhaf, H., Birk, M., Lange, A., Engel, A., Friedl-Vallon, F., Kirner, O., Kleinert, A., Maucher, G., Nordmeyer, H., Orphal, J., Ruhnke, R., Sinnhuber, B.-M., and Vogt, P.: Partitioning and budget of inorganic and organic chlorine species observed by MIPAS-B and TELIS in the Arctic in March 2011, Atmos. Chem. Phys., 15, 8065–8076, https://doi.org/10.5194/acp-15-8065-2015, 2015.

Wetzel, G., Oelhaf, H., Höpfner, M., Friedl-Vallon, F., Ebersoldt, A., Gulde, T., Kazarski, S., Kirner, O., Kleinert, A., Maucher, G., Nordmeyer, H., Orphal, J., Ruhnke, R., and Sinnhuber, B.-M.: Diurnal variations of $BrONO_2$ observed by MIPAS-B at midlatitudes and in the Arctic, Atmos. Chem. Phys., 17, 14631–14643, https://doi.org/10.5194/acp-17-14631-2017, 2017.

Wetzel, G., Friedl-Vallon, F., Glatthor, N., Grooß, J.-U., Gulde, T., Höpfner, M., Johansson, S., Khosrawi, F., Kirner, O., Kleinert, A., Kretschmer, E., Maucher, G., Nordmeyer, H., Oelhaf, H., Orphal, J., Piesch, C., Sinnhuber, B.-M., Ungermann, J., and Vogel, B.: Pollution trace gases C_2H_6, C_2H_2, HCOOH, and PAN in the North Atlantic UTLS: observations and simulations, Atmos. Chem. Phys., 21, 8213–8232, https://doi.org/10.5194/acp-21-8213-2021, 2021.

Wetzel, G., Höpfner, M., Oelhaf, H., Friedl-Vallon, F., Kleinert, A., Maucher, G., Sinnhuber, M., Abalichin, J., Dehn, A., and Raspollini, P.: Long-term validation of MIPAS ESA operational products using MIPAS-B measurements, Atmos. Meas. Tech., 15, 6669–6704, https://doi.org/10.5194/amt-15-6669-2022, 2022.

Wetzel, G., Kleinert, A., Johansson, S., Friedl-Vallon, F., Höpfner, M., Ungermann, J., Neubert, T., Catoire, V., Crevoisier, C., Engel, A., Gulde, T., Jacquet, P., Kirner, O., Kretschmer, E., Kulessa, T., Laube, J. C., Maucher, G., Nordmeyer, H., Piesch, C., Preusse, P., Retzlaff, M., Schardt, G., Schillings, J., Schneider, H., Schönfeld, A., Schuck, T., Woiwode, W., Riese, M., and Braesicke, P.: Intercomparison and validation of first GLORIA-B measurements of stratospheric and upper tropospheric long-lived tracers and photochemically active species, Atmos. Meas. Tech., 18, 5873–5894, https://doi.org/10.5194/amt-18-5873-2025, 2025.

Wiegele, A., Kleinert, A., Oelhaf, H., Ruhnke, R., Wetzel, G., Friedl-Vallon, F., Lengel, A., Maucher, G., Nordmeyer, H., and Fischer, H.: Spatio-temporal variations of NO_y species in the northern latitudes stratosphere measured with the balloon-borne MIPAS instrument, Atmos. Chem. Phys., 9, 1151–1163, https://doi.org/10.5194/acp-9-1151-2009, 2009.

https://doi.org/10.5194/egusphere-2026-5912
Preprint. Discussion started: 11 November 2026
© Author(s) 2026. CC BY 4.0 License.



WMO: Scientific assessment of ozone depletion: Global Ozone Research and Monitoring Project, GAW Report No. 278, Geneva, Switzerland: World Meteorological Organization, ISBN: 978-9914-733-97-6, 2022.

Xie, F., Tian, W., and Chipperfield, M. P.: Radiative effect of ozone change on stratosphere-troposphere exchange, J. Geophys. Res., 113, https://doi.org/10.1029/2008JD009829, 2008.

Zhu, Y., Mann, G., Newman, P. A., and Randel, W. (Eds.): APARC, 2025: The Hunga Volcanic Eruption Atmospheric Impacts Report, APARC Report No. 11, WCRP-10/2025, https://doi.org/10.34734/FZJ-2025-05237, 2025.